Bioactive macro/micro porous silk fibroin/nano-sized calcium phosphate scaffolds with potential for bone-tissue-engineering applications

Aim: The development of novel silk/nano-sized calcium phosphate (silk/nano-CaP) scaffolds with highly dispersed CaP nanoparticles in the silk fibroin (SF) matrix for bone tissue engineering. **Materials & methods:** Nano-CaP was incorporated in a concentrated aqueous SF solution (16 wt.%) by using an *in situ* synthesis method. The silk/nano-CaP scaffolds were then prepared through a combination of salt-leaching/lyophilization approaches. **Results:** The CaP particles presented good affinity to SF and their size was inferior to 200 nm when theoretical CaP/silk ratios were between 4 and 16 wt.%, as determined by scanning electron microscopy. The CaP particles displayed a uniform distribution in the scaffolds at both microscopic and macroscopic scales as observed by backscattered scanning electron microscopy and micro-computed tomography, respectively. The prepared scaffolds presented self-mineralization capability and no cytotoxicity confirmed by *in vitro* bioactivity tests and cell viability assays, respectively. **Conclusion:** These results indicated that the produced silk/nano-CaP scaffolds could be suitable candidates for bone-tissue-engineering applications.

KEYWORDS: bone tissue engineering ■ nanocomposite ■ nano-sized calcium phosphate ■ porous scaffold ■ silk fibroin

Le-Ping Yan[1,2],
Joana Silva-Correia[1,2],
Cristina Correia[1,2],
Sofia G Caridade[1,2],
Emanuel M Fernandes[1,2],
Rui A Sousa[1,2],
João F Mano[1,2],
Joaquim M Oliveira[1,2],
Ana L Oliveira[1,2,3] &
Rui L Reis*[1,2]

[1]*Biomaterials, Biodegradables & Biomimetics, University of Minho, Headquarters of the European Institute of Excellence on Tissue Engineering & Regenerative Medicine, AvePark, S. Cláudio de Barco, 4806-909 Taipas, Guimarães, Portugal*
[2]*ICVS/3B's - PT Government Associate Laboratory, Braga/Guimarães, Portugal*
[3]*Department of Health Sciences, Portuguese Catholic University, 3504-505 Viseu, Portugal*
*Author for correspondence:
Tel.: +351 253 510 900
Fax: +351 253 510 909
rgreis@dep.uminho.pt*

Bone tissue engineering requires the development of three-dimensional porous scaffolds with osteogenic properties [1]. Calcium phosphate-based (CaP) inorganic components have shown their osteogenesis potential in bone regeneration [2,3]. However, the fragile nature and slow degradation profile limit the application of these ceramic scaffolds. Combining natural or synthetic polymer with calcium phosphate is a promising strategy for bone-tissue-engineering scaffolding. A great deal of degradable polymers have been explored for this purpose [4]. Among those, silk fibroin (SF), derived from the silkworm *Bombyx mori*, has been considered as a versatile biomaterial for tissue-engineering applications [5–13].

Regarding the preparation of silk/CaP composite scaffolds, there are some challenging issues that need to be resolved. For instance, it is crucial to achieve good affinity between SF and CaP particles, as well as to maintain the porous structure and mechanical properties of the scaffold. On the other hand, the aggregation of CaP particles in the scaffold must be prevented. Furthermore, it is also important to achieve homogeneous distribution of the CaP particles inside the scaffold, both at macroscopic and microscopic scales. Many attempts have been made to improve the interface compatibility of the two phases in the scaffolds. Oliveira *et al.* synthesized hydroxyapatite (HA) in SF by the addition of phosphate ions into the calcium chloride/ethanol/water solution with dissolved SF [14]. This strategy allowed the formation of nano-sized HA inside the SF matrix. Kim *et al.* prepared aqueous-derived salt-leached SF scaffolds with the addition of polyaspartic acid, followed by the consecutive immersion of the scaffolds in calcium chloride and sodium phosphate monobasic solutions in order to form calcium phosphate crystal on the surface of the scaffolds [15]. The introduction of polyaspartic acid compromised the mechanical properties of the scaffolds. Collins *et al.* prepared the first load-bearing silk/CaP scaffold via an integrated procedure [16]. The generated scaffold presented mechanical properties comparable with cancellous bone, and a pore size range between 50 and 100 μm. In another interesting work, Zhang *et al.* tried to improve distribution homogeneity of the CaP particle in the scaffold by using the silk/CaP hybrid particle instead of the pure CaP particle [17]. Actually, it was shown that the CaP/silk composite scaffold enhanced the osteogenic differentiation of human bone mesenchymal stromal cells and promoted the cancellous bone formation in calvarial defect in SCID mice. However, the compressive strength of the scaffolds was less than 80 kPa. The above-mentioned studies somehow solved one or more challenges in the preparation of silk/CaP scaffolds, but had not yet reached the ideal level.

Future Medicine part of fsg

In a previous study, we have developed porous SF scaffolds with superior mechanical properties by using highly concentrated aqueous SF solution, via salt-leaching/freeze-drying methods [18]. In this study, we aim to solve the above-mentioned challenges by the introduction of nano-sized CaP in SF via an *in situ* synthesis method, followed by preparation of the porous scaffolds through salt-leaching/freeze-drying approaches. The structural conformations of SF and CaP were investigated by Fourier transform infra-red spectroscopy (FTIR) and/or x-ray diffraction (XRD) analysis. The morphology and microstructure of the silk/nano-CaP scaffolds were evaluated by scanning electron microscopy (SEM) and micro-computed tomography (micro-CT). The CaP content and Ca/P ratio in the scaffold were determined by thermal gravimetric analysis (TGA) and energy dispersive x-ray detector (EDX), respectively. The size and the microscopic distribution of the CaP nanoparticles were also investigated by backscattered SEM. The macroscopic distribution of the CaP nanoparticles in the scaffold was analyzed by micro-CT. The mechanical properties in dry state and wet state were characterized by compressive tests and dynamic mechanical analysis (DMA) at pH 7.4 and 37°C, respectively. Additionally, the hydration degree was registered from 3 h up to 30 days, and the weight loss was recorded from 1 up to 30 days. Finally, the cytotoxicity of the silk/nano-CaP scaffolds, along with the silk control scaffolds, were evaluated by carrying out a cellular viability test (by a 3-(4,5-dimethylthiazol-2-yl)-5-(3-carboxymethoxyphenyl)-2-(4-sulfophynyl)-2H-tetr-azolium) assay [MTS]) using mouse lung fibroblasts (L929 cell line) cells, which were previously in contact with the scaffolds' extract fluids.

Materials & methods
■ Materials
Cocoons of *B. mori* were offered by the Portuguese Association of Parents and Friends of Mentally Disabled Citizens (APPACDM, Portugal). In this study, sodium chloride particles (Portugal) of commercial grade were used. Silicone tubing (9 mm inner diameter) was obtained from Deltalab (Barcelona, Spain). The other materials and reagents were supplied by Sigma-Aldrich (MO, USA) unless mentioned otherwise.

■ Preparation of high-concentration SF aqueous solution

B. mori SF was extracted from cocoons as reported previously with slight modifications [12]. Briefly, the sericin was eliminated by boiling the cocoons for 1 h in 0.02 M sodium carbonate solution, and then rinsing thoroughly with distilled water. The purified SF was dissolved in 9.3 M lithium bromide solution at 70°C for 1 h. Following this, the SF solution was dialyzed against distilled water by using a benzoylated dialysis tubing (MWCO: 2000) for a period of 2 days. Afterwards, the SF solution was concentrated by dialysis in a 20 wt.% poly(ethylene glycol) solution (20,000 g/mol) for 6 h [19]. Finally, the tubing was carefully rinsed in distilled water, and the concentrated solution was collected. The concentration of the final SF solution was calculated by dividing the dry weight by the initial weight of the SF solution. The concentrated SF solution was kept at 4°C before use.

■ Preparation of salt-leached silk/nano-CaP scaffolds
Silk/nano-CaP composite was prepared via an *in situ* synthesis method. At first, the concentrated SF aqueous solution was diluted to 16 wt.%. Different amounts of a calcium chloride solution (6 mol/l) were mixed with the SF solution, followed by the addition of different amounts of an ammonia dibasic phosphate solution (3.6 mol/l). The theoretical calcium to phosphate atomic ratio was maintained at 1.67 in each group. The pH value of the system was adjusted to 8.5 by the addition of ammonia (30%). The suspension was stirred for 30 min and subsequently aged for 24 h at room temperature. The theoretical content of the CaP formed in the SF solution was determined based on the hypothesis that the calcium and phosphate species would react completely to form stoichiometric HA (HA), $Ca_{10}(PO)_6(OH)_2$. Silk/nano-CaP composites possessing a theoretical CaP content (theoretical CaP mass divided by the total mass of SF) of 4, 8, 16 and 25 wt.% were prepared. Fractions of sodium chloride particles having a size in the range of 500–1000 μm were obtained by using an analytical sieve shaker (Retsch, Haan, Germany). The silk/nano-CaP scaffolds were prepared by addition of 2.0 g of sodium chloride granule (500–1000 μm) to 1 ml silk/nano-CaP suspension, in a silicone tubing of 9 mm inner diameter, followed by drying the material inside the silicone tubing at room temperature for 2 days. Sodium chloride and the by-products were removed by immersion in distilled water for 2 days. The skin of the silk/nano-CaP scaffolds

was removed by a stainless steel punch of 6 mm inner diameter. Finally, the scaffolds were frozen at -80°C followed by lyophilization in a freeze-drier (Telstar/Cryodos/80, Terrassa, Spain). The prepared silk/nano-CaP scaffolds were designated as silk/CaP-4, silk/CaP-8, silk/CaP-16 and silk/CaP-25, according to their initially incorporated amount of CaP, respectively (Figure 1). The SF scaffolds (control) without CaP were also prepared from a 16 wt.% aqueous solution following our previously reported method [18].

■ Characterization of the physicochemical properties

XRD
The crystallinity of the silk/nano-CaP scaffolds on powder was investigated using an x-ray diffractometer (Philips PW 1710, The Netherlands) with Cu-Kα radiation (λ = 0.154056 nm). Data was collected from 0 to 60° 2θ values, and the step width and counting time were set at 0.02° and 2 s per step, respectively. The analysis was repeated twice for each formulation.

FTIR
The silk/nano-CaP scaffolds were first reduced to powder by using a mortar. The powders were mixed with potassium bromide (1:100, wt%) and then uniaxially pressed to obtain a transparent disk. The infrared spectra were obtained by FTIR (Perkin-Elmer 1600 series equipment, MA, USA), between 4000 to 500 cm^{-1}. Spectra were recorded at a resolution of 4 cm^{-1} with 32 scans. Each formulation was screened three times.

SEM
The cross-sectional morphology of the control scaffold and silk/nano-CaP scaffolds were observed under SEM (NanoSEM-FEI Nova 200, OR, USA). Prior to the analysis, the specimens were coated with Au/Pd SC502-314B in a high vacuum evaporator coater (E 6700, Quorum/Polaron, East Grinstead, UK). The size and the microscopic distribution of the CaP particle in the silk/nano-CaP scaffolds were determined. For the purpose of this study, silk/nano-CaP scaffolds were milled into powder followed by observation of the CaP particles in the composite powder via backscattered SEM (NanoSEM-FEI Nova 200) without any coating. The calcium and phosphate content in the powder was investigated by EDX during the SEM observation.

CaP content & Ca/P atomic ratio in the silk/nano-CaP scaffolds
The CaP content in the silk/nano-CaP scaffolds was determined by TGA (TGA Q500, TA Instruments, DE, USA). Each specimen was placed in a platinum pan and equilibrated at 50°C for 2 min, followed by increasing the temperature to 700°C at a rate of 20°C/min in
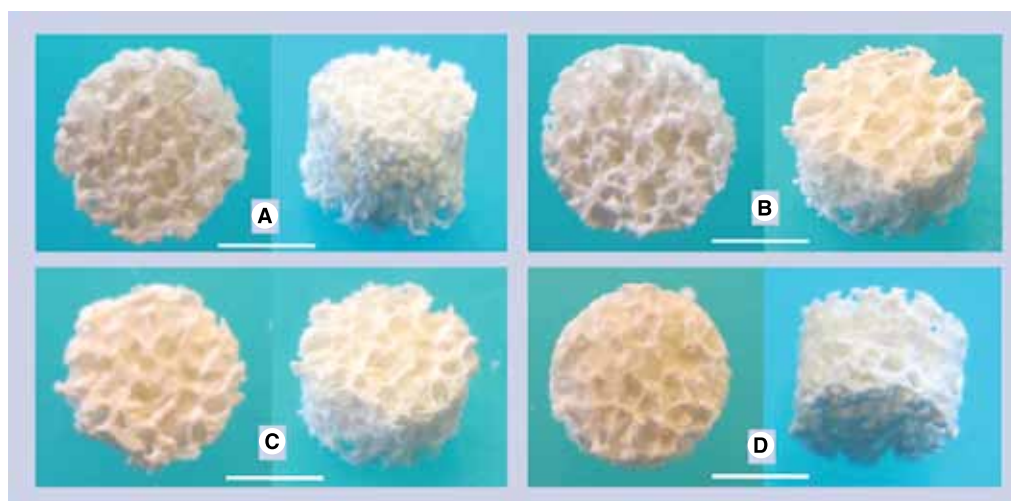
Figure 1. Macroscopic images of the silk/nano-sized calcium phosphate scaffolds.
(A) Silk/CaP-4, **(B)** silk/CaP-8, **(C)** silk/CaP-16 and **(D)** silk/CaP-25. Scale bar: 3 mm.
Silk/nano-CaP: Scaffolds composed of silk fibroin and nano-sized calcium phosphate; silk/CaP-4: Silk/nano-CaP scaffold with 4 wt.% initially theoretically incorporated CaP (divided by the mass of silk fibroin); silk/CaP-8: Silk/nano-CaP scaffold with 8 wt.% initially theoretically incorporated CaP (divided by the mass of silk fibroin); silk/CaP-16: Silk/nano-CaP scaffold with 16 wt.% initially theoretically incorporated CaP (divided by the mass of silk fibroin); silk/CaP-25: Silk/nano-CaP scaffold with 25 wt.% initially theoretically incorporated CaP (divided by the mass of silk fibroin).

air atmosphere. The CaP content in the scaffolds (CaP mass divided by the mass of SF) and the CaP incorporation efficiency were determined using Equations 1 & 2, respectively:

$$CaP\ content = [m_r/(m_i - m_r)] \times 100\%$$

(Equation 1)

$$CaP\ incorporation\ efficiency = (CaP\ content/theoretical\ CaP\ content) \times 100\%$$

(Equation 2)

The m_r is the weight of the residual, and the m_i is the initial weight of the scaffolds. The theoretical contents for silk/CaP-4, silk/CaP-8, silk/CaP-16 and silk/CaP-25 are 4, 8, 16 and 25 wt.%, respectively. Three specimens were evaluated for each formulation.

For the determination of the Ca/P atomic ratio in the scaffold, the silk/nano-CaP scaffolds were burned at 700ºC for 40 min in a furnace (Fornoceramica, Leiria, Portugal) to remove the SF. The obtained residual CaP was adhered in a cooper support for the analysis of the Ca/P atomic ratio by EDX (NanoSEM-FEI Nova 200). In each condition, five independent areas (200 × 200 µm) of the residual CaP were selected.

Micro-CT

The microstructure of the silk/nano-CaP scaffolds was qualitatively and quantitatively investigated by employing a high-resolution µ-CT (1072 scanner, SkyScan, Kontich, Belgium) possessing a resolution of pixel size of ~6.7 µm and time of integration of 1.3 s. The x-ray source was fixed at 61 keV and 163 µA. Around 300 projections were obtained over a 180º rotation with a step width of 0.45º. Data sets were rebuilt employing standardized software (NRecon v1.4.3, SkyScan) in a cone-beam model. The format of the output for each specimen was 300 serial bitmap images with 1024 × 1024 pixels. Representative serial images in each dataset were transferred into binary images by using grey values (dynamic threshold) of 40–255. Finally, the binary images were used for microstructrual analysis (CT Analyser, version 1.5.1.5, SkyScan), and to establish the 3D models (ANT 3D creator, version 2.4, SkyScan). At least three specimens were used for each condition. The macroscopic distribution of CaP in the silk/nano-CaP scaffolds was also assessed by micro-CT. The test followed the same procedure as mentioned above, but the dynamic threshold was set between 120 and 255 (grey values).

Mechanical properties
Compressive tests (dry state)
The tests were conducted in an unconfined mode by using a Universal Testing Machine (Instron 4505) with a load cell of 1 kN and at ambient temperature. The height and the diameter of the tested specimens were measured by a micrometer. The length and diameter of the tested specimens were approximately 6.50 mm and 5.30 mm, respectively. The cross-head speed was fixed at 2 mm/min and until 60% deformation in specimen height. The elastic modulus (E) was obtained from the slope of the initial linear domain of the stress–strain curve. The compressive strength was determined when the scaffold crushed. At least seven specimens for each formulation were tested.

DMA (wet state)
The viscoelastic mechanical properties of the scaffolds were measured by TRITEC8000B DMA (Triton Technology, UK) in a compressive mode. Scaffolds (cylindrical shape with 6 mm diameter and 4 mm thickness) were kept in a phosphate-buffered saline solution (PBS) at 37°C overnight. Afterwards, the specimens were fixed in the DMA apparatus and kept immersed in the PBS solution during the measurement. After reaching the equilibrium at 37ºC, the DMA spectra were recorded during a frequency sweep, ranging from 0.1 up to 25 Hz. Constant strain amplitude of 50 µm was used in all the experiments. Before the test, a small amount of preload was applied to each specimen to allow the complete contact of the scaffold surface with the compression plates. The distance between the plates was the same for all the tested scaffolds. A minimum of four samples was used for each formulation.

Hydration degree & weight loss ratio
The hydration degree (time period: 3 h until 30 days) and degradation behavior (time period: 1 to 30 days) of the silk/nano-CaP scaffolds were assessed after immersion into an 0.154 M sodium chloride isotonic saline solution (ISS, pH 7.4) [18]. These experiments were conducted at 37°C and dynamic condition (60 rpm) in a water bath (GFL 1086). At the end of each time point, the specimen was removed from the ISS and the wet weight was measured immediately after removing the excess surface water by using a filter paper. The hydration degree was calculated using Equation 3:

$$\text{Hydration degree} = [(m_{w,t} - m_0)/m_0] \times 100\%$$
(EQUATION 3)

where m_0 is the initial weight of the sample before hydration, and $m_{w,t}$ is the wet weight of the sample at time t after being removed from the ISS.

After the determination of the hydration degree, the specimens were rinsed with distilled water several times and dried in an oven at 60ºC for 24 h. The weight loss ratio was determined using EQUATION 4:

$$\text{Weight loss ratio} = [(m_0 - m_{d,t})/m_0] \times 100\%$$
(EQUATION 4)

where $m_{d,t}$ is the dry weight of the specimen being immersed in ISS for a certain time, and after drying at 60ºC for 24 h. Five specimens were measured for each formulation.

In vitro mineralization

The silk/nano-CaP scaffolds were immersed in a simulated body fluid (SBF) [20] solution for 7 days in an oven at 37ºC, following the method proposed by Kokubo *et al.* and adapted by Oliveira *et al.* [20,21]. At each timepoint, the specimens were removed from the SBF and washed by distilled water. The samples were frozen at -80ºC and lyophilized (Telstar/Cryodos/80, Spain). Then, the surfaces of the samples were analyzed by SEM and EDX (NanoSEM-FEI Nova 200). Prior to the SEM and EDX analysis, the samples were coated with carbon in a high vacuum evaporator coater (E 6700, Quorum/Polaron). For the EDX analysis, the data were collected by scanning three independent areas (5 × 5 μm) in each specimen for 90 s. Three specimens were analyzed in each assay for each group of scaffolds.

In vitro cytotoxicity screening

A 3-(4,5-dimethylthiazol-2-yl)-5-(3-carboxymethoxyphenyl)-2-(4-sulfophynyl)-2H-tetrazolium) (MTS) assay was performed to evaluate cytotoxicity of the silk/CaP-16 and silk control scaffold in comparison to latex (positive control for cell death), in accordance with ISO/EN 10993 (1992) Part 5 guidelines. Mouse lung fibroblasts (L929 cell line) were cultured as a monolayer in a Dulbecco's modified Eagle's medium (DMEM) supplemented with 10% fetal bovine serum (FBS, Biochrom, Berlin, Germany), 1% of antibiotic–antimycotic mixture (Invitrogen, USA) containing 10,000 U/ml penicillin G sodium, 10 mg/ml streptomycin sulfate and 25 μg/ml amphotericin B as Fungizone® (E.R. Squibb & Sons, NJ, USA) antimycotic in 0.85% saline. The L929 cells were incubated in an atmosphere containing 5% CO_2 at 37°C, with the medium changed every 2 days.

The extract fluids were prepared as previously reported by Oliveira *et al.* [21]. Briefly, extract fluids were obtained by immersing 1 g of scaffolds (sterilized by autoclave) in 50 ml tubes containing 20 ml complete DMEM culture medium. The tubes were incubated in a water bath at 37°C and 60 rpm for 24 h. A latex rubber extract was used as a positive control. Afterwards, the extract fluids were filtrated by using a 0.45 μm filter. Confluent L929 cells were detached from the culture flasks using trypsin (0.25% trypsin–EDTA solution) and a diluted cell suspension was prepared. The cells were seeded in a 96-well tissue culture polystyrene (TCPS) plate (six replicates per sample) at a cell density of 20,000 cells/well and incubated for 24 h at 37°C in an atmosphere with 5% CO_2. The culture medium in each well was removed and replaced by an identical volume (200 μl) of the extraction fluids. Cell culture medium was used as negative control. After 1, 3 and 7 days, the extracts were removed and replaced by 300 μl of mixed solution containing serum-free culture medium (without phenol red) and MTS (CellTiter 96 One Solution Cell Proliferation Assay Kit, Promega, PA, USA). After incubation for 3 h at 37°C in an atmosphere with 5% CO_2, the optical density (OD) was measured at 490 nm using a plate reader (Molecular Devices, CA, USA). Cell viability was calculated by subtracting the mean OD value of the blank (MTS solution) from the ones of the scaffolds and controls, followed by normalization with the mean OD value obtained for the negative control (cell culture medium). The MTS assay was performed in triplicate (n = 18).

■ Statistical analysis

All data were presented as average and standard deviation. A one-way analysis of variance (ANOVA) was used to assess the data obtained from TGA analysis, micro-CT analysis, compressive tests and cytotoxicity test. The comparison between two average values was evaluated using Tukey's test with $p < 0.05$ as statistical significance.

Results

■ Chemical structure

FIGURE 2A shows the XRD patterns of the silk
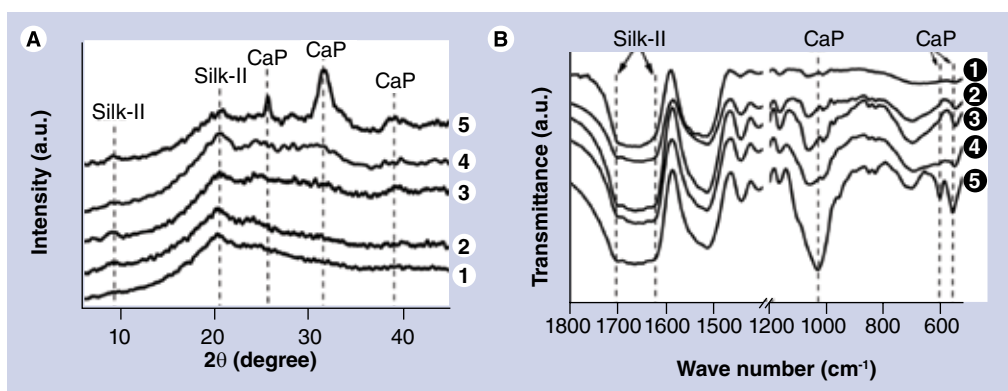
Figure 2. X-ray diffraction patterns (A) and Fourier transform infra-red spectroscopy spectra (B) of the silk and silk/nano-CaP scaffolds. (1) Control, **(2)** silk/CaP-4; **(3)** silk/CaP-8; **(4)** silk/CaP-16; **(5)** silk/CaP-25.
Silk/nano-CaP: Scaffolds composed of silk fibroin and nano-sized calcium phosphate. initially theoretically incorporated CaP (divided by the mass of silk fibroin); silk/CaP-4: Silk/nano-CaP scaffold with 8 wt.% initially theoretically incorporated CaP (divided by the mass of silk fibroin); silk/CaP-8: Silk/nano-CaP scaffold with 8 wt.% initially theoretically incorporated CaP (divided by the mass of silk fibroin); silk/CaP-16: Silk/nano-CaP scaffold with 16 wt.% initially theoretically incorporated CaP (divided by the mass of silk fibroin); silk/CaP-25: Silk/nano-CaP scaffold with 25 wt.% initially theoretically incorporated CaP (divided by the mass of silk fibroin).

and silk/nano-CaP porous scaffolds. The characteristic peaks of silk-II structure located at 9.0° and 20.5° were detected for all the scaffolds [12,19]. The broad peak width and low intensity of these two peaks indicate that the SF was of low crystallinity, comprising an uncertain amount of random coil. It was observed that as the amount of incorporated CaP increased, the intensity of the peaks located at 25.9°, 32.1° and 39.7° slightly increased. These peaks indicate that the CaP incorporated in the scaffold is a HA presenting low crystallinity [22]. The FTIR spectra (FIGURE 2B) corroborated the XRD analysis that revealed the conformation of silk-II in the SF in all the scaffolds. Peaks located at 1704 cm^{-1} and 1622 cm^{-1} can be attributed to silk-II [23,24]. The absorption area attributed to the v3 vibration of the PO_4^{3-} bond (between the absorption range of 970 cm^{-1} and 1100 cm^{-1}) increased with the increasing CaP content [17,21,25]. The v4 vibration of the PO_4^{3-} bond located at 607 cm^{-1} and 560 cm^{-1} [17,21,25] was distinct in the spectrum of silk/CaP-25, while the spectra of silk/CaP-4, silk/CaP-8 and silk/CaP-16 presented a lower intensity for this absorption. The XRD and FTIR results demonstrated that the CaP particles were successfully generated within the scaffolds.

■ Morphology & microstructure

FIGURE 3 shows SEM images of the different silk/nano-CaP scaffolds. All the scaffolds presented a macro/micro porous structure. The size of the macro-pores is around 500 µm, and

highly interconnected (FIGURE 3A, D, G & J). The trabeculae of the macro-pores were composed of partially interconnected micro-pores with a size ranging from 10 to 100 µm (FIGURE 3B, E, H & K). An interesting finding is the formation of cauliflower-like apatite clusters on the surface of silk/CaP-25, with a size around 700 nm (FIGURE 3L, inserted image). The clusters are composed of flake-like and worm-like apatite crystal.

The microstructure of the control and the silk/nano-CaP scaffolds was qualitatively and quantitatively studied by micro-CT (FIGURES 4 & 5). A highly porous structure was observed in all the silk/nano-CaP scaffolds from the two-dimensional and three-dimensional micro-CT images (FIGURE 4). From the three-dimensional micro-CT images, it is also possible to observe that the macro-pores are interconnected. Silk/CaP-4 possessed the highest porosity in the trabeculae of the macro-pores as compared with the other groups (FIGURE 4A–D). The two-dimensional micro-CT images also confirmed this observation (FIGURE 4E–H). FIGURE 5A shows that silk/CaP-4 presented the highest mean porosity (77.61 ± 0.72%), while silk/CaP-16 exhibited the lowest one (63.56 ± 2.43%) among the silk/nano-CaP scaffolds. The representative porosity distribution profile (FIGURE 5B) shows that a homogeneous porosity was observed for all the scaffolds. FIGURE 5C demonstrates that all the scaffolds presented interconnectivities higher than 70%. Silk/CaP-4 and silk/CaP-8 presented higher interconnectivity as compared to silk/CaP-16 and silk/CaP-25. The control

possessed higher porosity and interconnectivity as compared to all the silk/nano-CaP scaffolds.

■ Characterization of the CaP in the scaffold

TABLE 1 shows the CaP content and the incorporation efficiency for the different silk/nano-CaP scaffolds. After the extraction of sodium chloride particles, the CaP content was measured by TGA. This result demonstrated that most of the CaP formed was retained in the silk/CaP-8 and silk/CaP-16 as compared to silk/CaP-4 and silk/CaP-25. The Ca/P atomic ratio determined by EDX analysis is also shown in TABLE 1. The Ca/P atomic ratio was approximately 1.67 for all the silk/nano-CaP scaffolds, indicating the CaP synthesized in SF is similar to HA with respect to its chemical composition.

The backscattered SEM was used to identify the CaP particles and observe their microscopic distribution in the silk/nano-CaP composite powder based on the contrast differences of each element. EDX was employed to confirm the presence of the CaP particles together with backscattered SEM. The amount of CaP particles (white regions) in the composite powder increased when increasing the amount of initially incorporated CaP in the SF (FIGURE 6A–H). The size of the CaP particles in silk/CaP-4, silk/CaP-8 and silk/CaP-16 was inferior to 200 nm. Despite this, it was possible to observe particles with a size close to 1 µm in silk/CaP-25. The distribution of the CaP particles in silk/CaP-8, silk/CaP-16 and silk/CaP-25 was uniform at a microscopic scale (FIGURE 6C–H). The EDX spectra (FIGURE 6I–L) also showed that the CaP particles observed in the silk/nano-CaP scaffolds were generated without any by-product present – i.e., no chloride (from ammonia chloride and sodium chloride) and sodium ions (from sodium chloride) were detected. The CaP particles were well integrated into the SF matrix (FIGURE 6M & N).

Micro-CT analysis was performed in order to determine the distribution of CaP particles in the different silk/nano-CaP scaffolds. The sole CaP distribution profile (FIGURE 7A) shows that the CaP content (vol. %) increased from silk/CaP-4 to silk/CaP-16, and the distribution of CaP in the silk/nano-CaP scaffolds was homogeneous in each group. The combined SF and CaP distribution profile (FIGURE 7B) revealed that CaP content increased from silk/CaP-4 to silk/CaP-16, and the CaP presented homogeneous distribution at a macroscopic
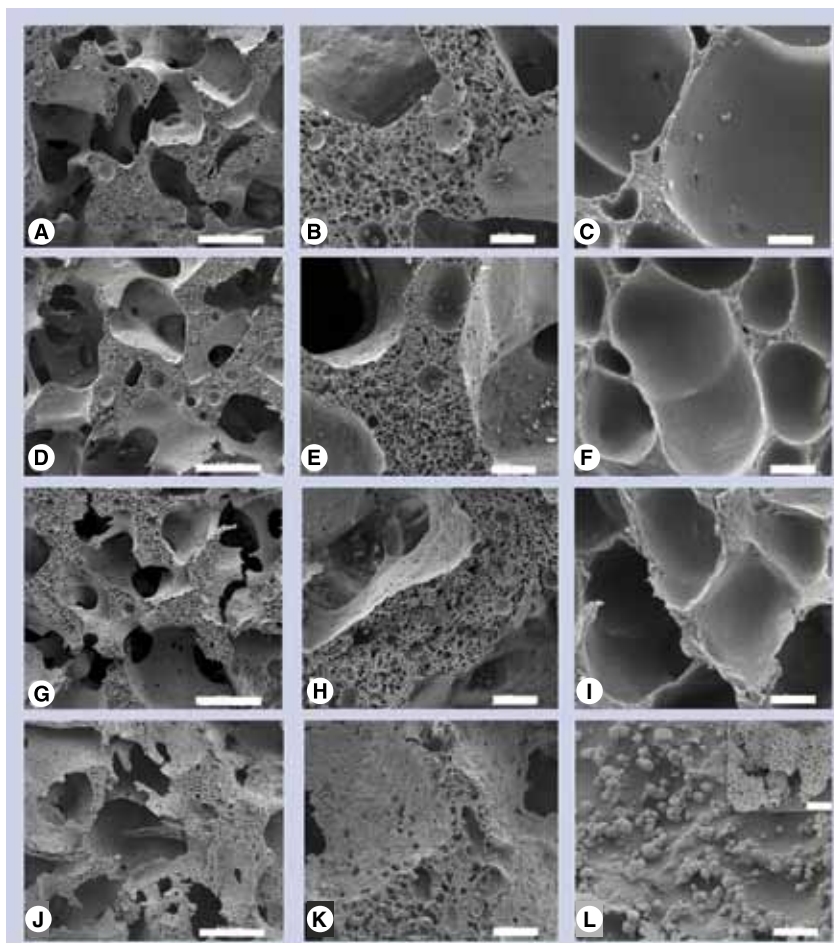
Figure 3. Morphology of the silk/nano-sized calcium phosphate scaffolds determined by scanning electron microscopy. (A), **(D)**, **(G)** and **(J)**: overview of silk/CaP-4, silk/CaP-8, silk/CaP-16 and silk/CaP-25, respectively (scale bar: 500 µm); **(B)**, **(E)**, **(H)** and **(K)**: trabecular structure of silk/CaP-4, silk/CaP-8, silk/CaP-16 and silk/CaP-25, respectively (scale bar: 100 µm); **(C)**, **(F)**, **(I)** and **(L)**: surface of the micro-pores of silk/CaP-4, silk/CaP-8, silk/CaP-16 and silk/CaP-25, respectively (scale bar: 5 µm). The inserted image in **(L)** is the amplified image of **(L)**, scale bar: 500 nm.
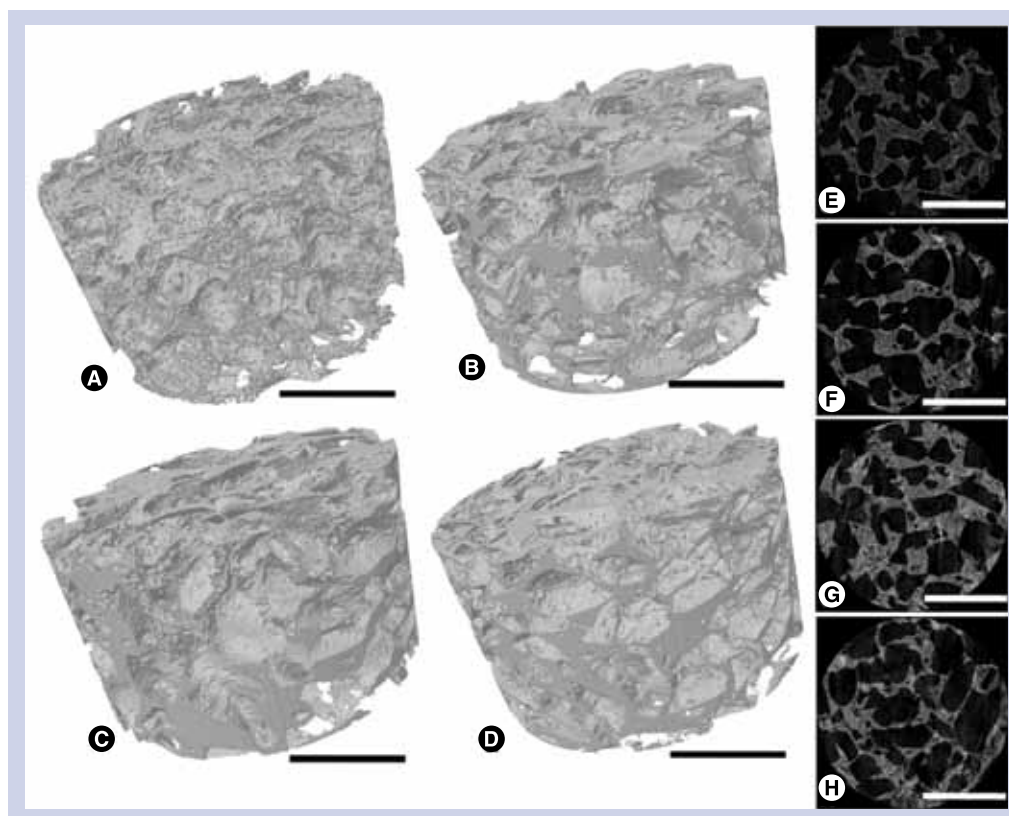Silk/nano-CaP: Scaffolds composed of silk fibroin and nano-sized calcium phosphate; silk/CaP-4: Silk/nano-CaP scaffold with 4 wt.% initially theoretically incorporated CaP (divided by the mass of silk fibroin); silk/CaP-8: Silk/nano-CaP scaffold with 8 wt.% initially theoretically incorporated CaP (divided by the mass of silk fibroin); silk/CaP-16: Silk/nano-CaP scaffold with 16 wt.% initially theoretically incorporated CaP (divided by the mass of silk fibroin); silk/CaP-25: Silk/nano-CaP scaffold with 25 wt.% initially theoretically incorporated CaP (divided by the mass of silk fibroin).

scale.

■ Mechanical properties

FIGURE 8 shows the compressive mechanical properties of the control and different silk/nano-CaP scaffolds determined in dry conditions. The values of the compressive modulus (FIGURE 8A) were 15.14 ± 1.70 MPa, 16.76 ± 4.58 MPa, 13.75 ± 2.99 MPa, 19.02 ± 5.77 MPa and 4.87 ± 0.95 MPa for the control, silk/CaP-4, silk/CaP-8, silk/CaP-16 and silk/CaP-25, respectively. The values of the compressive strength (FIGURE 8B) were

Figure 4. Micro-computed tomography three-dimensional images of (A) silk/CaP-4, (B) silk/CaP-8, (C) silk/CaP-16, and (D) silk/CaP-25silk scaffolds and respective two-dimensional images (E, F, G & H). Scale bar: 3 mm.
Silk/nano-CaP: Scaffolds composed of silk fibroin and nano-sized calcium phosphate; silk/CaP-4: Silk/nano-CaP scaffold with 4 wt.% initially theoretically incorporated CaP (divided by the mass of silk fibroin); silk/CaP-8: Silk/nano-CaP scaffold with 8 wt.% initially theoretically incorporated CaP (divided by the mass of silk fibroin); silk/CaP-16: Silk/nano-CaP scaffold with 16 wt.% initially theoretically incorporated CaP (divided by the mass of silk fibroin); silk/CaP-25: Silk/nano-CaP scaffold with 25 wt.% initially theoretically incorporated CaP (divided by the mass of silk fibroin).

0.69 ± 0.12 MPa, 0.59 ± 0.14 MPa, 0.63 ± 0.11 MPa, 0.62 ± 0.11 MPa and 0.25 ± 0.03 MPa for the control, silk/CaP-4, silk/CaP-8, silk/CaP-16 and silk/CaP-25, respectively. Regarding the compressive modulus and strength, there were no significant differences among the control, silk/CaP-4, silk/CaP-8 and silk/CaP-16.

The dynamic mechanical properties (wet conditions) of the control and different silk/nano-CaP scaffolds were also assessed by DMA (Figure 9). The storage modulus (E') of silk/CaP-4, silk/CaP-8 and silk/CaP-16 increased with the increasing of tested frequency (from 0.1 Hz to 25 Hz), while the E' for silk/CaP-25 presented no significant differences in all the tested frequencies. When the CaP content increased from 4% up to 16%, the storage modulus also increased for all the tested frequencies. Silk/CaP-16 presented the highest value in respect to storage modulus, which varied from 0.53 ± 0.15 MPa to 0.87 ± 0.12 MPa when the frequency increased from 0.1 Hz to 25 Hz. The loss factor (tan δ) of silk/CaP-4, silk/

CaP-8 and silk/CaP-16 were comprised between 0.16 and 0.2 when the tested frequency was inferior to 10 Hz.

■ **Hydration degree & weight loss ratio**
Figure 10 shows the hydration degree and weight loss ratio for the control and several silk/nano-CaP scaffolds. The hydration degree of each group scaffolds was maintained after immersion in sodium chloride solution after 6 h (Figure 10A). When increasing CaP content from 4 wt.% up to 16 wt.%, the hydration degree of the silk/nano-CaP scaffolds decreased after 6 h immersion. The hydration degree behavior of silk/CaP-25 was similar to silk/CaP-16 and the control. Regarding the weight loss profile, silk/CaP-4 presented the lowest weight loss ratio as compared to the other silk/nano-CaP scaffolds at day 1 and day 3 (Figure 10B). After 7 days of soaking, the weight loss value of all the silk/nano-CaP scaffolds presented no significant differences, while the control group presented

lower weight loss profile as compared with all the silk/nano-CaP scaffolds after immersion for 7 days.

In vitro mineralization

After immersion of the silk/nano-CaP scaffolds in SBF solution for 7 days, mineralized nuclei had grown on the surface of all the silk/nano-CaP scaffolds, as shown in FIGURE 11A–D. The EDX spectra confirmed that no other species than calcium and phosphorus have mineralized on the surface of the scaffolds (FIGURE 11E–H). The intensity of calcium and phosphorus signals increased from silk/CaP-4 to silk/CaP-25 (FIGURE 11E–H). Since EDX can detect elemental content under the surface up to 2 µm, the nano-CaP from the scaffolds might also contribute to the detected calcium and phosphorus signals. Further quantification analysis of the CaP minerals formed on the surface of the scaffolds should then be performed. The apatite minerals exhibited worm-like or flake-like morphology, with a size less than 500 nm (FIGURE 11A–D). It was also found that the minerals grew into cauliflower-like clusters, which were dominant in silk/CaP-25. This typical morphology has been described in previous studies [26], and results from the ability of a surface to induce *per se* the nucleation and growth of an apatite layer.

Cytotoxicity assessment

Latex leachables was used as control for cell death (positive control) in this study. This material has been described as cytotoxic and it has long been used [21] as control of cell death, in standard cytotoxicity assays. FIGURE 12 shows the cytotoxicity results of the silk control and silk/CaP-16. Cell viability of the silk control increased from day 1 to day 3 ($p < 0.05$), without significant difference between day 3 and day 7. Cell viability of silk/CaP-16 seemed to increase from day 1 to day 3, but without significant statistical difference. At day 7, silk/CaP-16 presented higher cell viability as compared to values obtained at day 1 and day 3, and as well as those of the silk control at all the tested time points. Furthermore, both silk control and silk/CaP-16 showed higher cell viability as compared to the negative control at day 3 and day 7. The positive control (latex) presented negative values in cell viability at all the tested time points ($p < 0.05$). The negative value (%) of the positive control was due to the OD value of the latex being lower than the one of the blank (MTS); thus, it would generate a negative value following the calculation procedure (see section
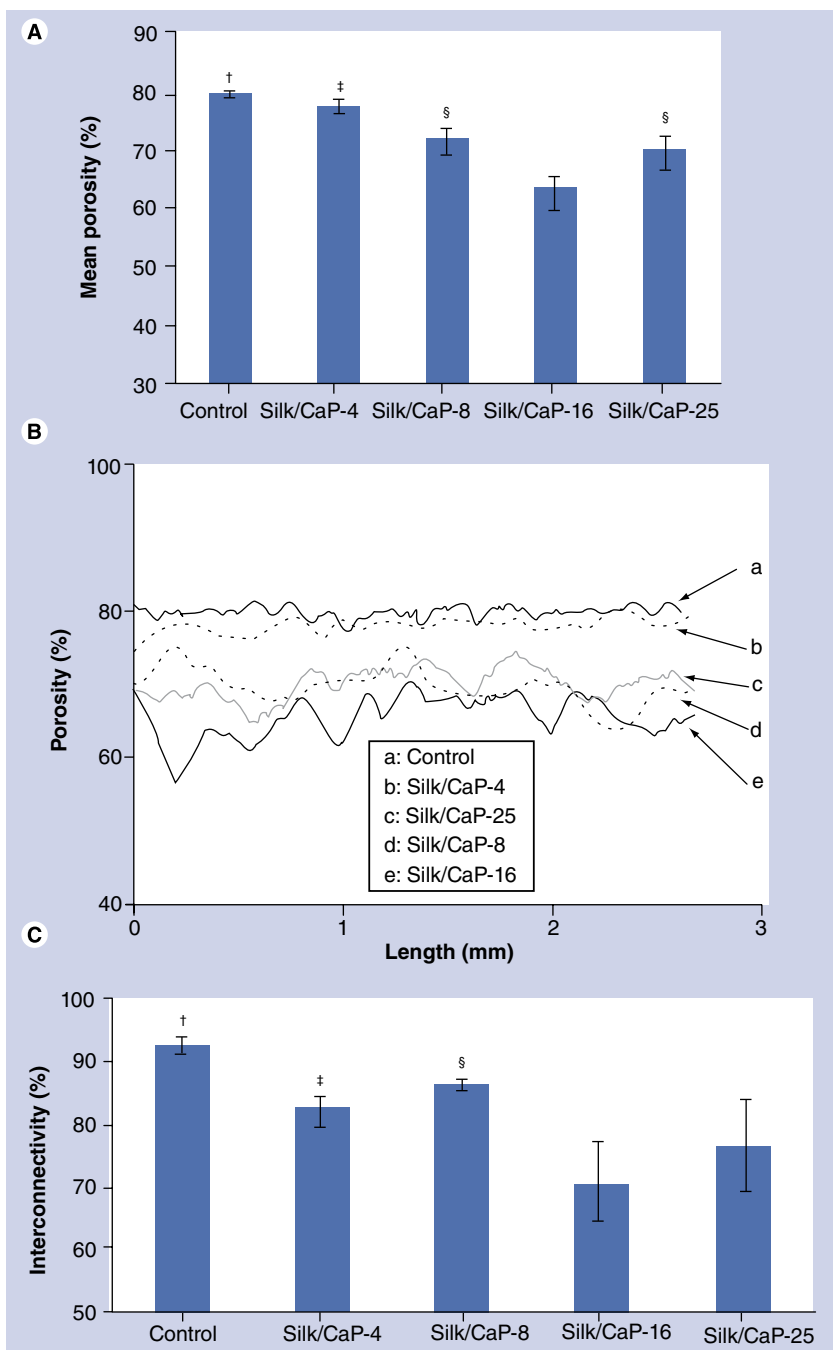
Figure 5. (A) Mean porosity, (B) representative porosity distribution along the length, and (C) interconnectivity of the silk/nano-sized calcium phosphate porous scaffolds determined by micro-computed tomography. (A) [†]indicates significant differences compared with silk/CaP-4, silk/CaP-8, silk/CaP-16 and silk/CaP-25; [‡]indicates significant differences compared with silk/CaP-8, silk/CaP-16 and silk/CaP-25; [§]indicates significant differences compared with silk/CaP-16. (C) [†]indicates significant differences compared with silk/CaP-4, silk/CaP-8, silk/CaP-16 and silk/CaP-25; [‡]indicates significant differences compared with silk/CaP-8 and silk/CaP-16; [§]indicates significant differences compared with silk/CaP-16. Silk/nano-CaP: Scaffolds composed of silk fibroin and nano-sized calcium phosphate; silk/CaP-4: Silk/nano-CaP scaffold with 4 wt.% initially theoretically incorporated CaP (divided by the mass of silk fibroin); silk/CaP-8: Silk/nano-CaP scaffold with 8 wt.% initially theoretically incorporated CaP (divided by the mass of silk fibroin); silk/CaP-16: Silk/nano-CaP scaffold with 16 wt.% initially theoretically incorporated CaP (divided by the mass of silk fibroin); silk/CaP-25: Silk/nano-CaP scaffold with 25 wt.% initially theoretically incorporated CaP (divided by the mass of silk fibroin).

Table 1. The calcium phosphate content, calcium phosphate incorporation efficiency and calcium/phosphate atomic ratio in the silk/nano-sized calcium phosphate scaffolds determined by thermal gravimetric and energy dispersive x-ray detector analyses.

Groups	Theoretical CaP content (wt%)[†]	Final CaP content (wt%)[‡]	CaP incorporation efficiency (%)[§]	Ca/P atomic ratio[¶]
Silk/CaP-4	4	2.57 ± 0.04	64.17 ± 0.88	1.66 ± 0.06
Silk/CaP-8	8	6.92 ± 0.35[#]	86.44 ± 4.44	1.68 ± 0.06
Silk/CaP-16	16	13.92 ± 0.76[††]	87.01 ± 4.72	1.67 ± 0.05
Silk/CaP-25	25	18.16 ± 1.00[‡‡]	72.63 ± 4.01	1.65 ± 0.03

[†]The theoretical CaP content was calculated based on the hypothesis that the added Ca and P ions would react completely and that the formed CaP would be $Ca_{10}(PO)_6(OH)_2$ (hydroxyapatite), which is the most stable phase under the processing conditions. The values were obtained by dividing the mass of the theoretical formed CaP by the mass of silk fibroin in each condition.
[‡]The final CaP content is determined by dividing the mass of residual CaP obtained from thermal gravimetric assay by the mass of silk fibroin (determined by total mass of the scaffold minus the mass of residual CaP).
[§]The CaP incorporation efficiency was calculated by dividing the final CaP content by the theoretical CaP content.
[¶]The Ca/P atomic ratio was determined by analysis of the CaP residual by energy dispersive x-ray detector analysis after burning the scaffolds in a furnace. In each condition, five independent areas (200 × 200 μm) of the CaP residual were selected for this assay.
[#]Significant difference compared with silk/CaP-4.
[††]Significant differences compared with silk/CaP-4 and silk/CaP-8.
[‡‡]Significant differences compared with silk/CaP-4, silk/CaP-8 and silk/CaP-16.
CaP: Calcium phosphate; Silk/nano-CaP: Scaffolds composed of silk fibroin and nano-sized calcium phosphate; silk/CaP-4: Silk/nano-CaP scaffold with 4 wt.% initially theoretically incorporated CaP (divided by the mass of silk fibroin); silk/CaP-8: Silk/nano-CaP scaffold with 8 wt.% initially theoretically incorporated CaP (divided by the mass of silk fibroin); silk/CaP-16: Silk/nano-CaP scaffold with 16 wt.% initially theoretically incorporated CaP (divided by the mass of silk fibroin); silk/CaP-25: silk/nano-CaP scaffold with 25 wt.% initially theoretically incorporated CaP (divided by the mass of silk fibroin).

'*In vitro* cytotoxicity screening' in Materials and Methods).

Discussion

In previous studies, porous silk/CaP scaffolds have shown promising potential in bone tissue engineering scaffolding [14–17,27]. However, a silk/CaP scaffold possessing suitable mechanical properties, proper microstructure and homogeneous distribution of the CaP particles to better match bone tissue engineering scaffolding demand has not yet been developed. Previously, macro-/micro-porous silk scaffolds with good mechanical properties and high interconnectivity were developed by means of using high-concentration aqueous SF solution (up to 16 wt.%) and a combination of salt-leaching/lyophilization approaches [18]. In the present study, we propose an *in situ* synthesis method for the formation of nano-sized CaP particles within the matrix of macro/micro porous SF scaffolds.

FIGURE 2 showed that the CaP particles were successfully incorporated in the SF scaffolds. The XRD analysis indicated that the incorporated CaP particles could be assigned to a low crystalline HA, which is of great biomedical relevance as it can mimic closer bone

apatite [23]. Dorozhkin reported that mixing the calcium and phosphate ions in aqueous solution would first form amorphous calcium phosphates, which were thermodynamically unstable compounds and spontaneously tended to transform into crystalline apatite [23]. In the present work, the CaP particles (amorphous CaP) were aged in the SF solution for 24 h (HA) prior to their incorporation into the SF scaffold. The XRD results show that the CaP did not change its structure during the salt-leaching in distilled water for 2 days. This result is consistent with the previous study [28], which studied the SF-regulated mineralization process of calcium phosphate. The XRD and FTIR results also indicate that the incorporation of CaP did not impair the formation of β-sheet conformation in the SF. The formation of β-sheet is critical for the maintenance of the mechanical properties and structural stability of the silk/nano-CaP scaffolds.

Kim *et al.* found that the addition of sodium chloride particles into SF solution would induce the formation of β-sheet conformation in the SF [12]. Based on this finding, they were able to generate aqueous-derived porous SF scaffolds. However, with this method, they only prepared SF scaffolds using aqueous SF solution with no
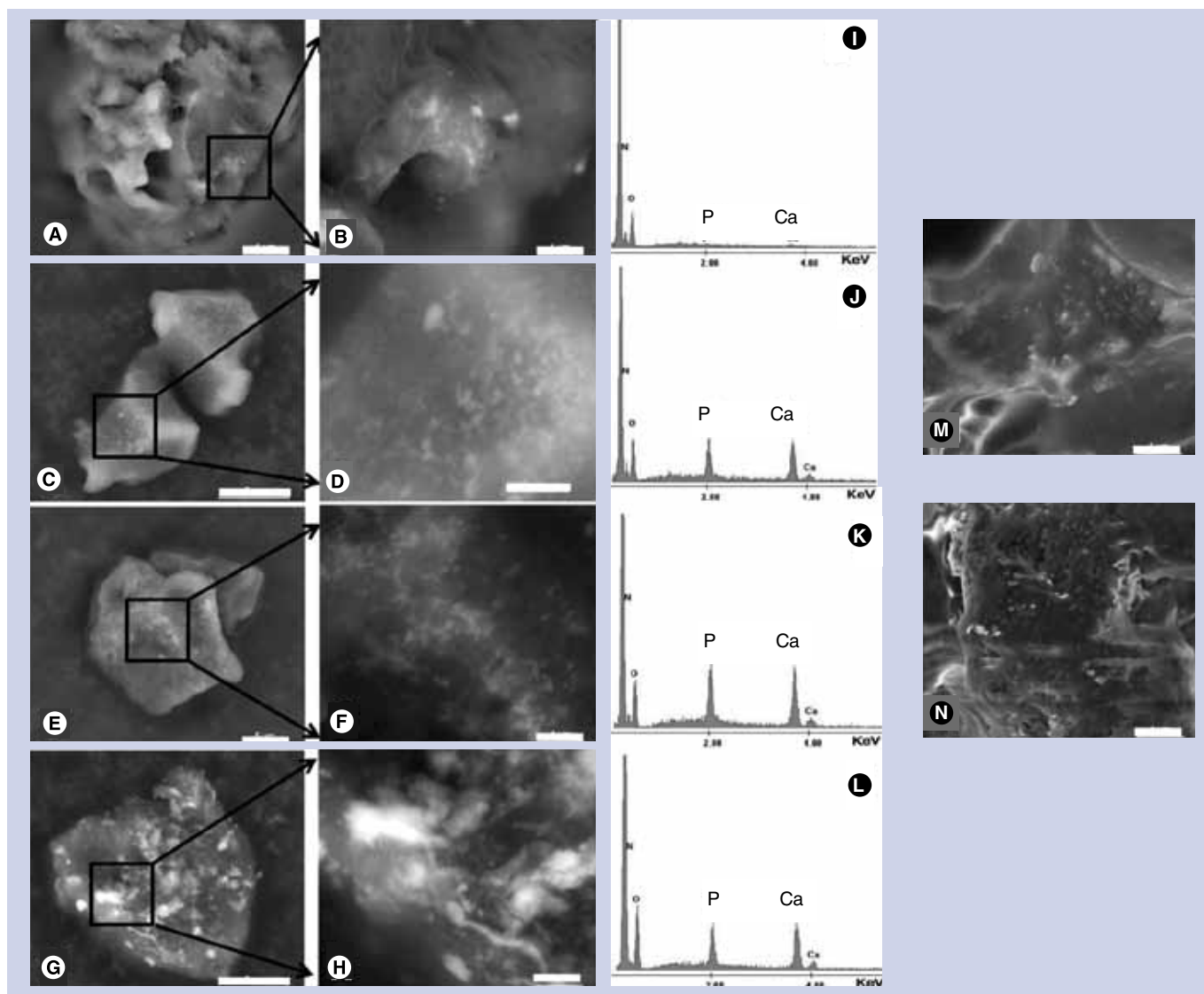
Figure 6. Distribution and particle size of the calcium phosphate particle in the silk/nano-sized calcium phosphate scaffolds determined by scanning electron microscopy and energy dispersive x-ray detector analysis. (A–H) were observed in a backscattered scanning electron microscopy (SEM) model, while **(M)** and **(N)** were observed in a secondary electron SEM model. **(A)**, **(C)**, **(E)** and **(G)**: SEM images for silk/CaP-4, silk/CaP-8, silk/CaP-16 and silk/CaP-25, respectively (scale bar: 5 µm). **(B)**, **(D)**, **(F)** and **(H)**: amplified SEM images of **(A)**, **(C)**, **(E)** and **(G)**, respectively (scale bar: 1 µm). **(M)** and **(N)**: secondary electron SEM images of **(D)** and **(F)**, respectively (scale bar: 1 µm). **(I)**, **(J)**, **(K)** and **(L)**: Energy dispersive x-ray detector spectra of **(B)**, **(D)**, **(F)** and **(H)**, respectively. CaP: Calcium phosphate; silk/nano-CaP: Scaffolds composed of silk fibroin and nano-sized calcium phosphate; silk/CaP-4: Silk/nano-CaP scaffold with 4 wt.% initially theoretically incorporated CaP (divided by the mass of silk fibroin); silk/CaP-8: Silk/nano-CaP scaffold with 8 wt.% initially theoretically incorporated CaP (divided by the mass of silk fibroin); silk/CaP-16: Silk/nano-CaP scaffold with 16 wt.% initially theoretically incorporated CaP (divided by the mass of silk fibroin); silk/CaP-25: Silk/nano-CaP scaffold with 25 wt.% initially theoretically incorporated CaP (divided by the mass of silk fibroin).

more than 10 wt.% concentration. In our recent study, it was shown that SF scaffold obtained combining salt-leaching and lyophilization methods can be prepared by using aqueous SF solution up to 16 wt.% [18]. In the present study, we demonstrated that the salt-leached porous silk/nano-CaP scaffolds derived from 16 wt.% SF aqueous solution can also be prepared by a similar approach (**FIGURES 1 & 3**). The SEM analysis of the silk/nano-CaP scaffolds revealed that the morphology of the silk/CaP-4, silk/CaP-8 and silk/CaP-16 was similar to that of pure SF scaffold (16 wt.%) [18]. The formation of the apatite crystals on the surface of silk/CaP-25 can occur during the extraction procedure. During the salt extraction, the CaP particles would partially dissolve in water, increasing the local concentration of calcium and phosphate ions. The local enrichment of calcium and phosphate ions was favorable for the nucleation of apatite on
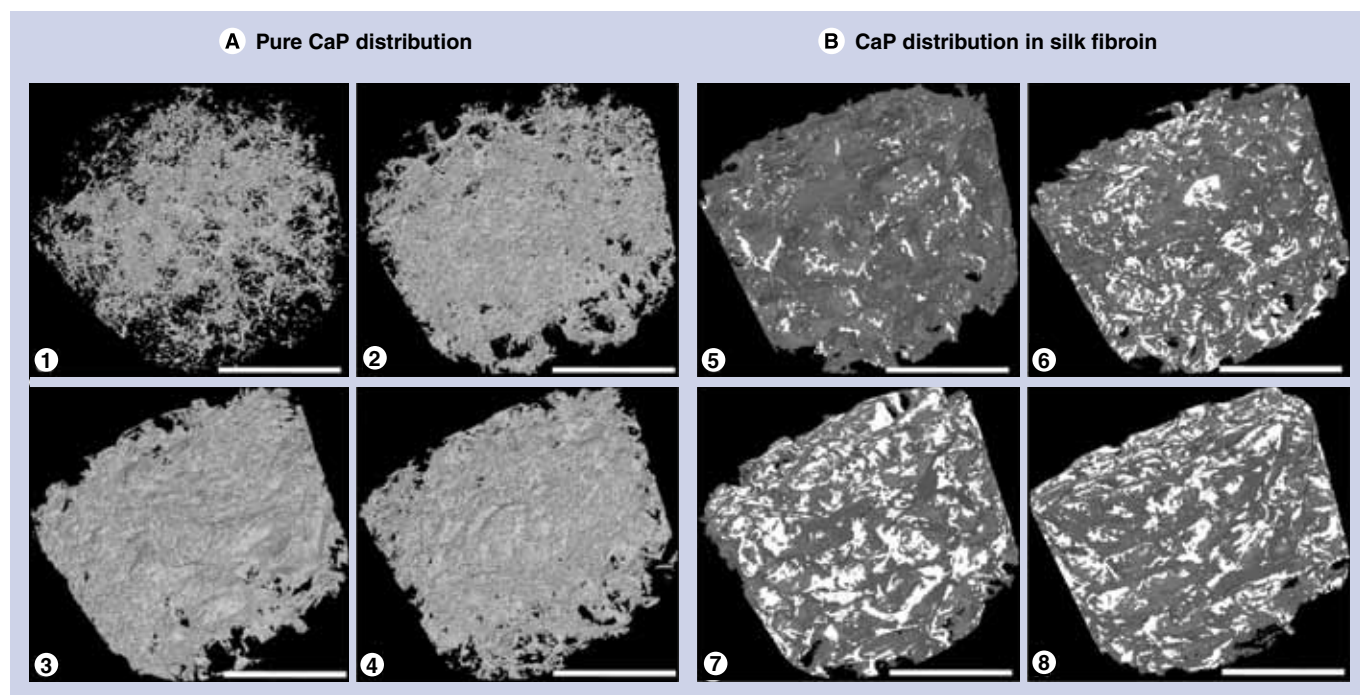
Figure 7. Three-dimensional images of pure calcium phosphate distribution and calcium phosphate distribution in silk fibrion in the silk/nano-sized calcium phosphate porous scaffolds, determined by micro-computed tomography.
In **(B)**, silk fibroin: the gray domain; CaP: the white domain. **(1)** and **(5)**: silk/CaP-4; **(2)** and **(6)**: silk/CaP-8; **(3)** and **(7)**: silk/CaP-16; **(4)** and **(8)**: silk/CaP-25 (scale bar: 3 mm).
CaP: Calcium phosphate; silk/nano-CaP: Scaffolds composed of silk fibroin and nano-sized calcium phosphate; silk/CaP-4: Silk/nano-CaP scaffold with 4 wt.% initially theoretically incorporated CaP (divided by the mass of silk fibroin); silk/CaP-8: Silk/nano-CaP scaffold with 8 wt.% initially theoretically incorporated CaP (divided by the mass of silk fibroin); silk/CaP-16: Silk/nano-CaP scaffold with 16 wt.% initially theoretically incorporated CaP (divided by the mass of silk fibroin); silk/CaP-25: Silk/nano-CaP scaffold with 25 wt.% initially theoretically incorporated CaP (divided by the mass of silk fibroin).

the surface of the scaffolds, similar to the process observed for the studies on the biomineralization of HA scaffolds in a stimulated body fluid [21]. The size of the macro-pores (around 500 µm) in all the silk/nano-CaP scaffolds is adequate for bone scaffolding, as it has been shown to support new bone formation and vascularization [29]. The size of the micro-pores in the silk/nano-CaP scaffolds is suitable for promoting the cell attachment and proliferation [29]. Furthermore, the macro-pores are highly interconnected (FIGURE 3), which would benefit cell ingrowth and tissue regeneration.

It has been shown that micro-CT is a powerful tool to quantitatively and qualitatively characterize the microstructure of scaffolds [30]. The observation from the three-dimensional and two-dimensional micro-CT images (FIGURE 4) corroborates the data obtained from the SEM images in respect to the morphology of scaffolds (FIGURE 3). Silk/CaP-4 possessed the lowest amount of CaP content as compared with the other groups; thus, its porosity (FIGURE 5A) is closest to that of the control [18]. As the initially incorporated content of the CaP increased from

4 wt.% to 16 wt.%, the total porosity of the scaffolds decreased (FIGURE 5). This is because the trabeculae of the macro-pores of the scaffolds were impregnated with increased CaP particles. Actually, this observation is supported by the data obtained from micro-CT analysis (FIGURE 4). As the initially incorporated CaP content increased up to 25 wt.%, silk/CaP-25 presented lower structural integrity compared with other groups (FIGURES 3, 8 & 9), and thus induced a higher porosity as compared with silk/CaP-16 (FIGURE 5A). Moreover, it was also observed that the distribution of the porosity along the scaffold is homogenous in all the groups (FIGURE 5B), and the interconnectivity remained at a high level (FIGURE 5C), indicating that the incorporation of CaP particles did not affect the foreseen architecture of the scaffolds.

The SF retained a large amount of the initially incorporated CaP in the scaffolds (TABLE 1) within the SF matrix. The highly concentrated SF aqueous solution played an important role in preventing the leaching out of the CaP particles from the scaffolds. In our previous study [18], it was found that the thickness of the trabeculae of
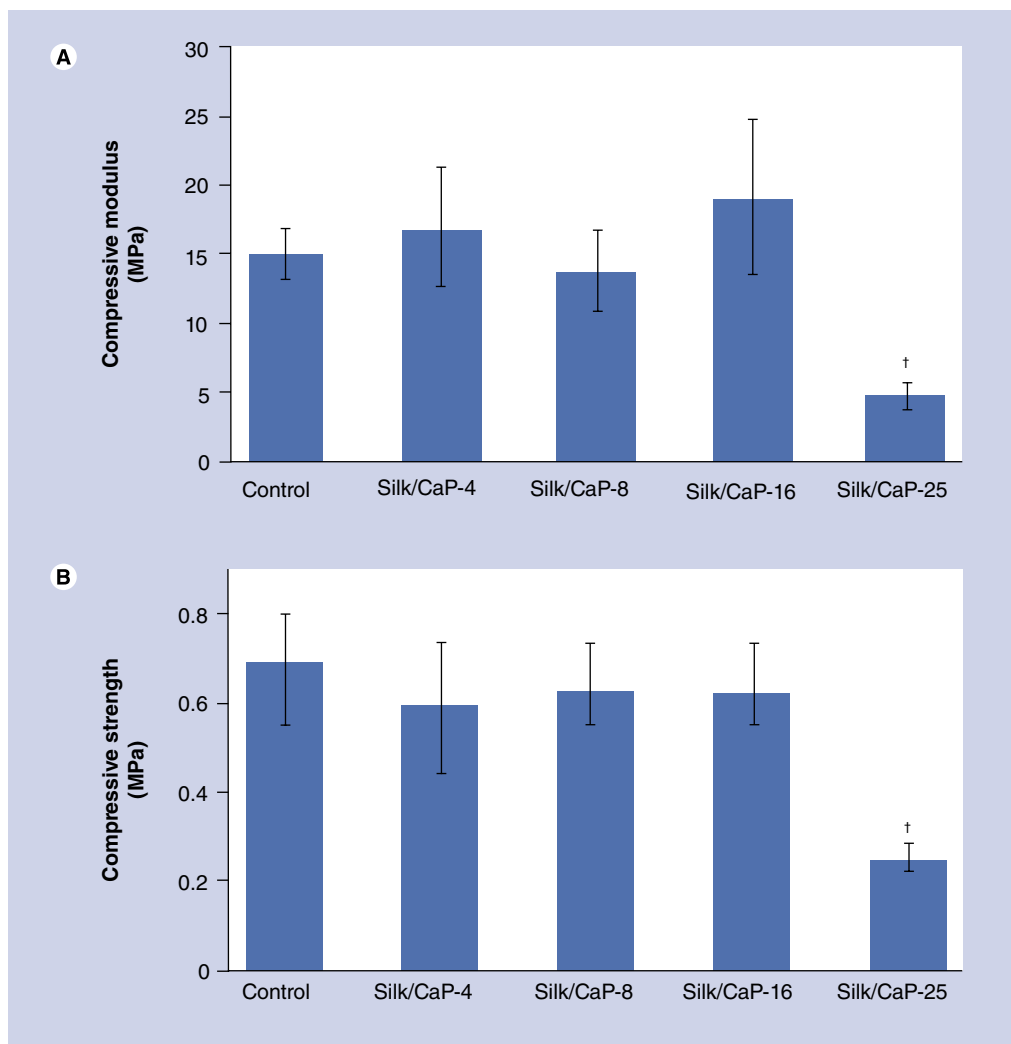
Figure 8. (A) Compressive modulus and (B) compressive strength of the silk and silk/nano-sized calcium phosphate scaffolds. [†]indicates significant differences compared with silk/CaP-4, silk/CaP-8 and silk/CaP-16.

Silk/nano-CaP: Scaffolds composed of silk fibroin and nano-sized calcium phosphate; silk/CaP-4: Silk/nano-CaP scaffold with 4 wt.% initially theoretically incorporated CaP (divided by the mass of silk fibroin); silk/CaP-8: Silk/nano-CaP scaffold with 8 wt.% initially theoretically incorporated CaP (divided by the mass of silk fibroin); silk/CaP-16: Silk/nano-CaP scaffold with 16 wt.% initially theoretically incorporated CaP (divided by the mass of silk fibroin); silk/CaP-25: Silk/nano-CaP scaffold with 25 wt.% initially theoretically incorporated CaP (divided by the mass of silk fibroin).

the macro-pores in the salt-leached SF scaffolds increase with the increase of SF concentration, being higher for scaffolds derived from 16 wt.% SF solutions. We observed that the thicker the trabeculae thickness, the higher the amount of CaP can be retained in the scaffolds (data not shown). This justifies the use of a highly concentrated SF aqueous solution in this study. It should be addressed that the CaP vol.% shown in FIGURE 7, cannot represent the real CaP particle content in each group of scaffolds. This is due to the fact that the resolution of the micro-CT equipment used in this study is 6 µm. Since the size of most of the CaP particles is less than

1 µm, it is impossible to quantitatively determine the CaP content in the silk/nano-CaP scaffolds by micro-CT. A similar observation has been reported in previous studies; Oliveira *et al.* quantified the biomimetic CaP coating by micro-CT for the first time [30]. It was found that the micro-CT equipment was still capable of detecting the CaP coating – even the thickness of the biomimetic CaP coating was around 8 µm and the resolution of the micro-CT instrument was 11 µm, due to the high diffraction of the ceramic when comparing with the polymer. This observation was consistent with the result in this study (FIGURE 7). On the other hand,
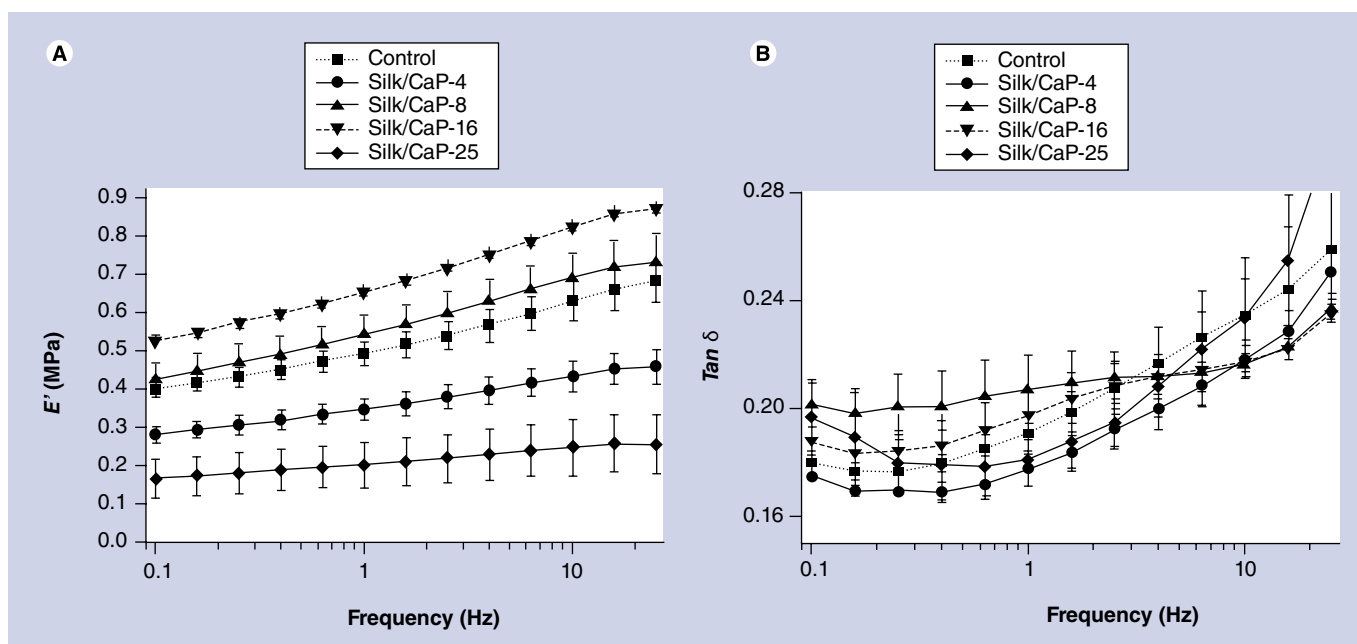
Figure 9. (A) Storage modulus and (B) loss factor of the silk and silk/nano-sized calcium phosphate scaffolds determined by dynamic mechanical analysis at 37°C in phosphate-buffered saline solution.
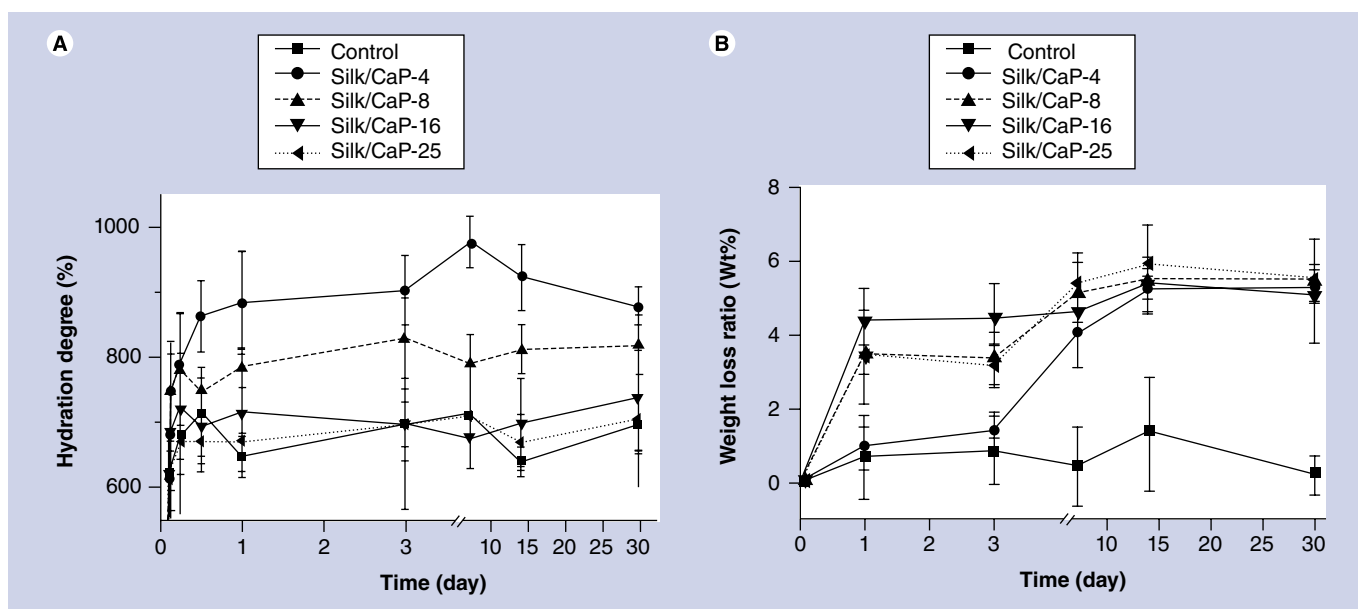Silk/nano-CaP: Scaffolds composed of silk fibroin and nano-sized calcium phosphate; silk/CaP-4: Silk/nano-CaP scaffold with 4 wt.% initially theoretically incorporated CaP (divided by the mass of silk fibroin); silk/CaP-8: Silk/nano-CaP scaffold with 8 wt.% initially theoretically incorporated CaP (divided by the mass of silk fibroin); silk/CaP-16: Silk/nano-CaP scaffold with 16 wt.% initially theoretically incorporated CaP (divided by the mass of silk fibroin); silk/CaP-25: Silk/nano-CaP scaffold with 25 wt.% initially theoretically incorporated CaP (divided by the mass of silk fibroin).

Bhumiratana *et al.* also found that not all the HA micro-particles were detected by micro-CT, since the resolution of micro-CT (21 μm) is a little higher than the approximate size of HA (20 μm) [27]. That is the reason why we used TGA to quantitatively evaluate the CaP content of the silk/nano-CaP scaffolds. On the other hand, the formed CaP presented a Ca/P atomic ratio close to 1.67, which is in good agreement with the initial Ca/P atomic ratio (TABLE 1), and corresponds to the value calculated for stoichiometric HA.

A previous study by Kong *et al.* has shown that the *in situ* synthesis approach allowed for the formation of nano-sized HA crystal in the diluted SF solution (less than 2 wt.%) [28]. However, with low-concentration SF solution, it is difficult to generate a mechanical stable porous scaffold [14]. In this study, we performed, for the first time, the synthesis of nano-sized CaP particles in highly concentrated SF solution by an *in situ* synthesis method. Our approach allowed the development of SF scaffolds with good mechanical properties and generattion of nano-sized CaP particles in the scaffold. It was reported that the nano-sized particles tend to aggregate and precipitate due to the electrostatic interaction [17]. Our preliminary result also showed that the CaP particles would precipitate at the bottom when aqueous SF solutions of low concentration were used (data not shown). The backscattered SEM images confirmed that the nano-sized CaP presented a homogeneous distribution, without aggregation, in the SF matrix at a microscopic scale (FIGURE 6). Furthermore, the CaP particles were homogeneously distributed in all the silk/nano-CaP scaffolds, at a macroscopic scale (FIGURE 7). It can be concluded that the highly concentrated SF aqueous solution had prevented the aggregation and the precipitation of the nano-size CaP particles in the composite system.

A homogeneous distribution of nano-sized or micro-sized CaP particles in the SF scaffold without aggregation is still very challenging. Liu *et al.* prepared silk/CaP scaffolds by physical mixture of SF and nano-sized HA particles in aqueous phase [31]. However, there was evidence that the nano-sized HA particles partially aggregated into micro-sized particles on the surface of the macro-pores in the scaffold. Bhumiratana *et al.* produced porous silk/CaP scaffolds by physically mixing the SF and micro-sized HA particles in organic phase [27]. From the SEM observations, it was found that the HA particles were partially aggregated at the surface of the scaffolds. Zhang *et al.* prepared silk/CaP porous scaffold from SF aqueous solution and

Figure 10. (A) Hydration degree and (B) weight loss ratio of the silk and silk/nano-sized calcium phosphate scaffolds determined by immersion in sodium chloride solution at 37°C (60 rpm) for different time periods.
Silk/nano-CaP: Scaffolds composed of silk fibroin and nano-sized calcium phosphate; silk/CaP-4: Silk/nano-CaP scaffold with 4 wt.% initially theoretically incorporated CaP (divided by the mass of silk fibroin); silk/CaP-8: Silk/nano-CaP scaffold with 8 wt.% initially theoretically incorporated CaP (divided by the mass of silk fibroin); silk/CaP-16: Silk/nano-CaP scaffold with 16 wt.% initially theoretically incorporated CaP (divided by the mass of silk fibroin); silk/CaP-25: Silk/nano-CaP scaffold with 25 wt.% initially theoretically incorporated CaP (divided by the mass of silk fibroin).

micro-sized CaP/silk hybrid particles [17]. The CaP/silk particles distributed homogenously at a macroscopic scale in the scaffold in their study. From the above-mentioned studies, it was found that it is feasible to achieve a homogeneous distribution of the CaP particles in SF scaffolds, but not at a microscopic scale. In the present study, the combination of an *in situ* synthesis method and highly concentrated SF aqueous solution was used to solve this challenge. Notably, this combination approach allowed the formation of nano-sized CaP particles and prevented the aggregation and precipitation of the CaP particles (FIGURE 6A–H). As a consequence, it allowed the homogeneous distribution of the nano-sized CaP particles in the silk/nano-CaP scaffolds, at both microscopic scale (FIGURE 6C–H) and macroscopic scales (FIGURE 7). The prepared silk/nano-CaP scaffolds were shown to comprise both homogeneous porosity and CaP particle distribution across the scaffolds, which is an advantage for tissue engineering scaffolding.

The mechanical performance of a scaffold plays an important role in tissue regeneration, especially when hard tissues are the targets, such as in the case of bone. The control of the mechanical properties of the scaffolds aiming at matching the mechanical environment of the host tissues has been a subject of great attention over the last years [16,32,33]. In this sense, we

have envisioned the use of high-concentration aqueous SF solution as a possible strategy to improve the mechanical properties of the SF scaffolds. Regarding the dry status properties of the silk/nano-CaP scaffolds, it is possible to state that the addition and increasing content of CaP particles in the SF scaffolds showed no statistical differences for the control, silk/CaP-4, silk/CaP-8 and silk/CaP-16 (FIGURE 8A & B), indicating that the nucleation and growth of the nano-sized CaP particles within the SF scaffolds did not compromise its dry-state mechanical performance in this study. The DMA data indicated that the control, silk/CaP-4, silk/CaP-8 and silk/CaP-16 possessed good elasticity and stable viscosity, as their storage modulus increased with the increase of the frequency, and their loss factors were between 1.6 and 0.2 (FIGURE 9). The storage modulus (wet state) of the silk/nano-CaP scaffolds presented porosity dependence when the initially incorporated CaP content was comprised between 4 and 16 wt.%. The storage modulus of silk/CaP-8 is comparable to that of the control, while silk/CaP-16 presented a higher value. These results demonstrated that the mechanical performance of the silk-based scaffolds (wet state) can be maintained or even improved after incorporation of a certain amount of nano-sized CaP in the salt-leached SF scaffolds.
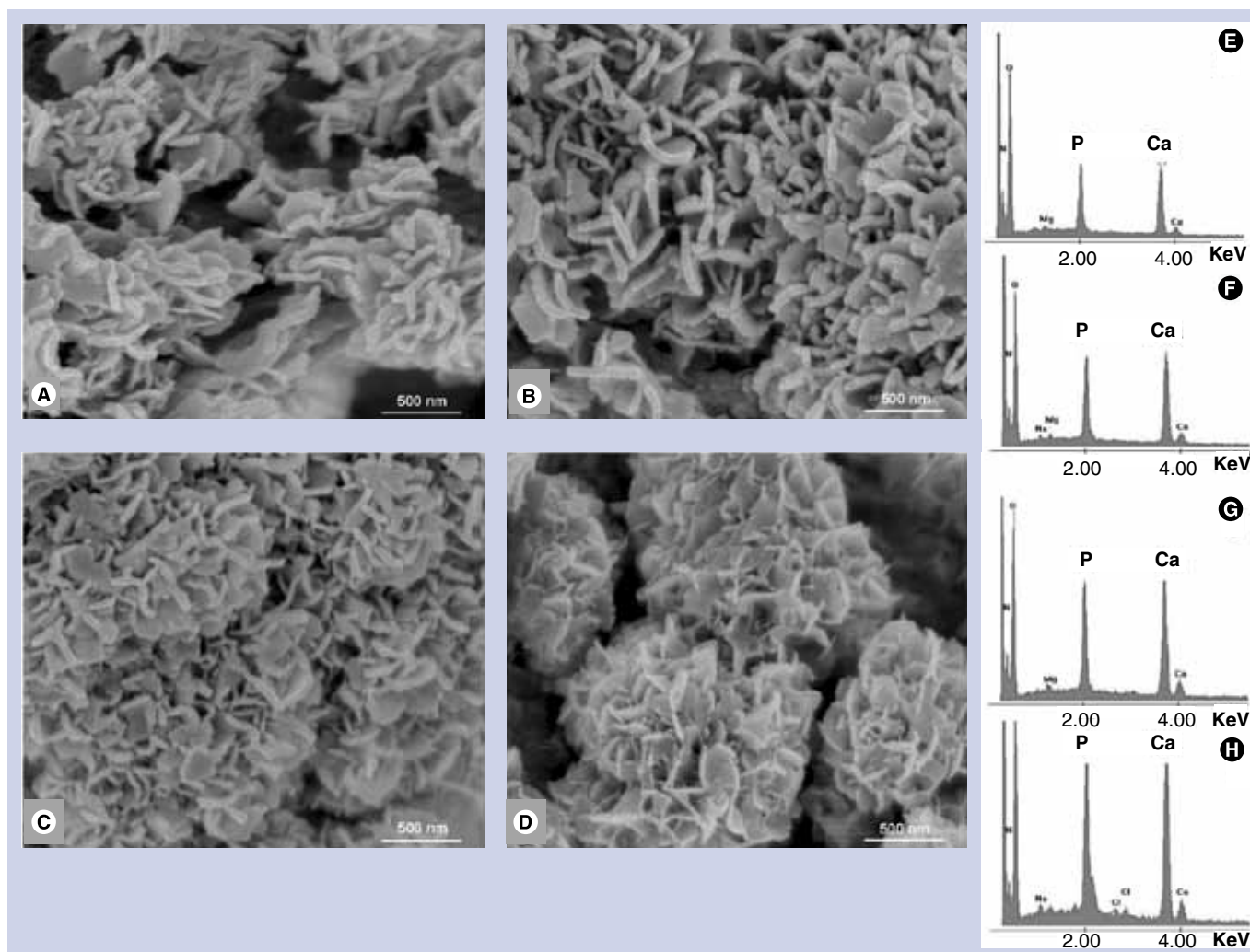
Figure 11. Mineralization of the silk/nano-sized calcium phosphate porous scaffolds determined by scanning electron microscopy and energy dispersive x-ray detector, after immersion in a simulated body fluid solution for 7 days.
(A), **(B)**, **(C)** and **(D)** are the scanning electron microscopy images of the mineral on the surface of silk/CaP-4, silk/CaP-8, silk/CaP-16 and silk/CaP-25, respectively. **(E)**, **(F)**, **(G)** and **(H)** are energy dispersive x-ray detector spectra corresponding to **(A)**, **(B)**, **(C)** and **(D)**, respectively.
Silk/nano-CaP: Scaffolds composed of silk fibroin and nano-sized calcium phosphate; silk/CaP-4: Silk/nano-CaP scaffold with 4 wt.% initially theoretically incorporated CaP (divided by the mass of silk fibroin); silk/CaP-8: Silk/nano-CaP scaffold with 8 wt.% initially theoretically incorporated CaP (divided by the mass of silk fibroin); silk/CaP-16: Silk/nano-CaP scaffold with 16 wt.% initially theoretically incorporated CaP (divided by the mass of silk fibroin); silk/CaP-25: Silk/nano-CaP scaffold with 25 wt.% initially theoretically incorporated CaP (divided by the mass of silk fibroin).

As compared with the mechanical properties of silk/CaP scaffolds reported from other studies, silk/CaP-16 prepared in this study possessed a compressive modulus of around 19 MPa, which is approximately five-times higher than the highest one reported by Liu *et al.* [31]. In their study, the highest compressive modulus of the silk/HA scaffolds was around 3.2 MPa. By its turn, the compressive modulus of silk/CaP-16 was around nine-times higher to that of the salt-leached SF scaffolds coated with a biomimetic CaP layer developed by Kim *et al.* [15]. The compressive modulus in that study was about 2 MPa. By comparing the compressive strength of silk/CaP-16 (0.62 MPa) to other studies, our value was around seven-times and three-times higher as compared with those reported by Zhang *et al.* [17] and Kim *et al.* [15], respectively. In their studies, the compressive strengths of the scaffolds were approximately 80 and 150 kPa, respectively. However, the mechanical properties of scaffolds prepared in this study are inferior as compared with cross-linked silk/CaP scaffolds reported by Collins *et al.* [16]. In their study, the chemical cross-linking was performed by using hexamethylene diisocyanate to endow the scaffolds with mechanical performance comparable to that of cancellous bone, with

an average compressive modulus of 175 MPa and strengths of 14 MPa. The size of the interconnected pores of those scaffolds was relatively lower (50–100 µm) compared with the one in this study (around 500 µm). The lower pore sizes may also be contributed to the outstanding mechanical performance of the silk/CaP scaffolds developed in their study. However, this approach is a little risky; the residual of the hexamethylene diisocyanate must be removed completely and the safety of the degradation products should also be investigated.

The hydration behavior and the degradation ratio of the scaffold are also critical to the cell attachment, proliferation and the final outcome of the regenerated tissue. The hydration ratio of the silk/nano-CaP scaffolds is related to the porosity and structure integrity. From silk/CaP-4 to silk/CaP-16, the hydration degree decreased as the porosity decreased (**Figure 10A & Figure 5A**). Since the integrity of silk/CaP-25 is lower as compared with the other groups (**Figure 3**), its ability to retain the water inside the scaffold also decreased (**Figure 10A**). The hydration degrees of silk/nano-CaP scaffolds demonstrated in this study were higher than those reported by Liu *et al.* [31]. In their study, the porosities of the silk/CaP scaffolds were between 41 and 61%, resulting in the lower hydration degrees. All the silk/nano-CaP scaffolds showed good stability, after 1 month of immersion in a sodium chloride solution. This result is related to the β-sheet conformation of the SF, which conferred good water stability to the silk/nano-CaP scaffolds. Actually, the degradation profiles of silk/nano-CaP scaffolds resemble that reported for the control SF scaffolds after immersion in ISS for 7 days [18]. Despite this, the slight weight loss of the silk/nano-CaP scaffolds can be directly related to the partial dissolution of the poorly crystalline CaP. In fact, small amounts of calcium and phosphate ions were detected in the degradation solution of the silk/nano-CaP scaffolds by ion-coupled plasma (data not shown), in a preliminary study. The systematic study of the degradation profile of CaP particles in the silk/nano-CaP scaffolds is presently ongoing. The release of calcium and phosphate ions from the silk/nano-CaP scaffolds is viewed as an advantage, as it would promote bone regeneration when applied for bone tissue engineering, as previously reported by Oliveira *et al.* [2,3], Zhang *et al.* [17] and Bhumiratana *et al.* [27].

An *in vitro* bioactivity test performed in SBF has been used to predict the *in vivo* bone
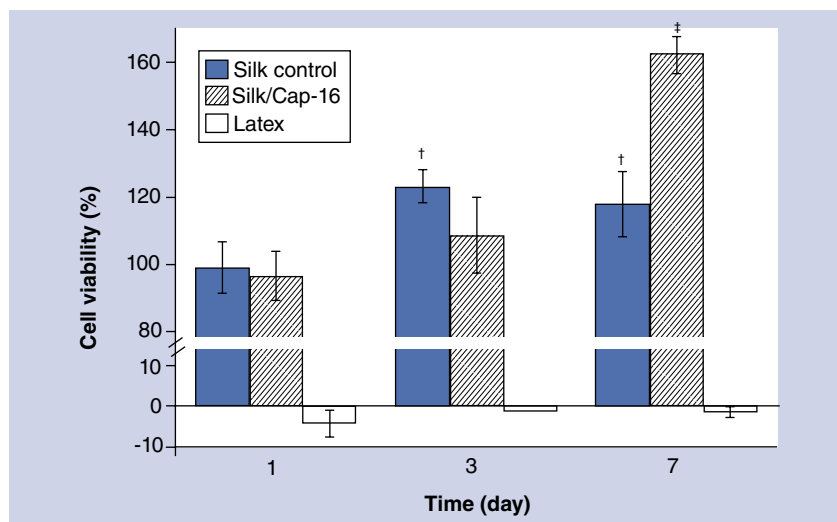
Figure 12. Cytotoxicity assessment of the leachables from control and silk/CaP-16 using L929 cells. †Indicates significant differences as compared with the cell viability at day 1; ‡indicates significant differences as compared to the cell viability of the control at all the tested time points, and as well as the cell viability of silk/CaP-16 at day 1 and day 3. Extract fluid of latex used as positive control. Silk/CaP-16: Silk/nano-CaP scaffold with 16 wt.% initially theoretically incorporated CaP (divided by the mass of silk fibroin).

bioactivity of biomaterials [20]. If a biomaterial can induce an apatite layer on its surface in SBF, it can probably bond to living bone *in vivo*. HA was found to be bioacitve both in SBF and *in vivo*. The formation of apatite on its surface in SBF was due to the dissolution of calcium and phosphate ions from HA [21]. In this study, nano-sized CaP particles were incorporated into the SF scaffolds. The low crystallinity nature of these CaP particles allowed the dissolution of calcium and phosphate ions in SBF solution, and subsequently induced the formation of apatite on the surface of the scaffolds. It was noticed that silk/nano-CaP scaffolds still presented bioactivity even when incorporated with a small amount of nano-sized CaP particles; for instance, silk/CaP-4. The bioactive nature of silk/nano-CaP scaffolds indicates that these scaffolds possess great potential for bone tissue engineering applications.

The assessment of the cytotoxicity of scaffolds by using their extract fluid has been investigated in our previous studies [21,25]. Since silk/CaP-16 presented higher mechanical performance (wet state) as compared with other silk/nano-CaP scaffolds, it was selected along with the control for the cytotoxicity test. The cell viability was over 100% in some data points, meaning that the leachables from the scaffolds can induce higher cell metabolic activity compared with normal culture medium. The leachables from the SF scaffold were probably composed of some small SF nanoparticles, which may act

as a nutrient source for the cells. Similarly, the leachables from the silk/nano-CaP scaffolds were almost certainly the nano-sized CaP/silk composite. The nano-sized particles released calcium and phosphate ions, as well as the SF fragments. These factors might be helpful to increase the cell's viability. The cell viability data clearly demonstrated that the silk/CaP-16 and the control presented no cytotoxicity, which means that there are no toxic traces remaining in the scaffolds. This data also validates the processing method for the macro/micro porous silk and silk/nano-CaP scaffolds.

Conclusion

In this study, macro/micro porous silk/nano-CaP scaffolds were produced, through the *in situ* synthesis of nano-sized CaP in a high-concentration aqueous SF solution (16 wt.%) followed by scaffolding using a salt-leaching/lyophilization approach. The CaP particles consisted of poorly crystalline HA and the SF presented β-sheet conformation. The synergetic effect of the *in situ* synthesis method and the highly concentrated SF aqueous solution allowed for uniform distribution of the CaP particles in the scaffolds, at both microscopic and macroscopic scales. The combination of salt-leaching/lyophilization approaches allowed the formation of highly interconnected macro-pores, homogeneous porosity distribution, and high interconnectivity in the silk/nano-CaP scaffolds. The silk/nano-CaP scaffolds with the theoretical CaP content of 16 wt.% present the highest wet status storage modulus. The porosity and hydration degree of the silk/nano-CaP scaffolds can be controlled by the amount of CaP particles incorporated. The developed silk and silk/nano-CaP scaffolds are noncytotoxic. The silk/nano-CaP scaffolds developed present promising mechanical properties, architecture and stability, bioactivity and no cytotoxicity, which make them suitable for possible application in bone tissue engineering scaffolding.

Future perspective

By combining the *in situ* synthesis method with the traditional scaffolding approaches, bioactive nanocomposite-based scaffold with homogeneous distribution of the nano-particles was achieved. The incorporation of nano-sized CaP particles will endow the SF scaffolds with the property of osteoconductivity. Besides that, much room remains for the development of multi-functional silk/nano-CaP scaffolds based on this study. The surface functionality of these scaffolds might be helpful to guide the cell attachment and migration. By using some green chemistries, such as plasma treatment and supercritical fluid processing, the surface chemistry and surface roughness can be tuned, and play an important role in cell behavior.

Executive summary

Bridging of nanoparticles with porous scaffold
- This study presented a good example of how to bridge the nano-sized bioactive particles with a three-dimensional porous scaffold by using combined facile approaches, namely *in situ* synthesis and salt-leaching/lyophilization.

Controlling the size of nano-sized calcium phosphate in silk fibroin
- Nano-sized calcium phosphate (CaP) particles were successfully synthesized *in situ* in a highly concentrated silk fibroin (SF) aqueous solution. The size of the synthesized CaP particles can be controlled at less than 200 nm by varying the amount of CaP incorporated in the SF solution.

Homogeneous distribution of nano-CaP
- The *in situ* synthesis method allowed the homogeneous distribution of the nano-sized CaP within the SF matrix, both at microscopic and macroscopic scales.

Superior mechanical properties
- The mechanical performance of the silk/nano-CaP scaffolds can be maintained or improved by the incorporation of different amounts of nano-sized CaP particles.

High interconnectivity
- The macro/micro porous structure, along with the high interconnectivity of the silk/nano-CaP scaffolds, make them promising scaffolds for bone tissue engineering.

Tunable physicochemical properties
- The porosity and the hydration degree can be tuned by the amount of CaP particles incorporated.

Osteogenesis potential
- All the silk/nano-CaP scaffolds developed in this study were able to induce the formation of apatite on their surface in simulated body fluid. The bioactivity of these scaffolds indicates that they possess osteoconductive properties and present osteogenesis potential, which is advantageous in bone tissue engineering.

Noncytotoxic
- The developed silk and silk/nano-CaP scaffolds are noncytotoxic.

Furthermore, the nano-CaP particles also present advantages for the affinity of bisphosphonates on their surface, such as alendronate and zoledronate. Combining the achievement of this study, it could even better enhance bone regeneration by loading these drugs in the nano-CaP particles during the *in situ* synthesis procedure and subsequently incorporating into the scaffolds. Other drugs, for instance water-soluble dexamethasone or antibiotics, could also be combined in the scaffolds by this manner, to improve the bone repair outcomes.

Ethical conduct of research
The authors state that they have obtained appropriate institutional review board approval or have followed the principles outlined in the Declaration of Helsinki for all human or animal experimental investigations. In addition, for investigations involving human subjects, informed consent has been obtained from the participants involved.

References
Papers of special note have been highlighted as:
- ▪ of interest
- ▪▪ of considerable interest

1   Hutmacher DW, Schantz JT, Lam CXF, Tan KC, Lim TC. State of the art and future directions of scaffold-based bone engineering from a biomaterials perspective. *J. Tissue Eng. Regen. M.* 1(4), 245–260 (2007).

2   Oliveira JM, Kotobuki N, Tadokoro M *et al.* *Ex vivo* culturing of stromal cells with dexamethasone-loaded carboxymethylchitosan/poly(amidoamine) dendrimer nanoparticles promotes ectopic bone formation. *Bone* 46(5), 1424–1435 (2010).

3   Oliveira JM, Sousa RA, Kotobuki N *et al.* The osteogenic differentiation of rat bone marrow stromal cells cultured with dexamethasone-loaded carboxymethylchitosan/poly(amidoamine) dendrimer nanoperticles. *Biomaterials* 30(5), 804–813 (2009).

4   Rezwan K, Chen QZ, Blaker JJ, Boccaccini AR. Biodegradable and bioactive porous polymer/inorganic composite scaffolds for bone tissue engineering. *Biomaterials* 27(18), 3413–3431 (2006).

5   Oliveira AL, Sun L, Kim HJ *et al.* Aligned silk-based 3-D architectures for contact guidance in tissue engineering. *Acta Biomater.* 8(4), 1530–1542 (2012).

6   Fuchs S, Jiang X, Schmidt H *et al.* Dynamic process involved in the pre-vascularization of silk fibroin constructs for bone regeneration using outgrowth endothelial cells. *Biomaterials* 30(7), 1329–1338 (2009).

7   Makaya K, Terada S, Ohgo K, Asakura T. Comparative study of silk fibroin porous scaffolds derived from salt/water and sucrose/hexafluoroisopropanol in cartilage formation. *J. Biosci. Bioeng.* 108(1), 68–75 (2009).

8   Vepari C, Kaplan DL. Silk as a biomaterial. *Prog. Polym. Sci.* 32(8–9), 991–1007 (2007).

▪   **Comprehensive review on the development of a diversity of silk-based scaffolds, as well as the modification and biological performance of these scaffolds.**

9   Kundu B, Kundu SC. Osteogenesis of human stem cells in silk biomaterial for regenerative therapy. *Prog. Polym. Sci.* 35(9), 1116–1127 (2010).

10   Bessa PC, Balmayor ER, Azevedo HS *et al.* Silk fibroin microparticles as carriers for delivery of human recombinant BMPs. Physical characterization and drug release. *J. Tissue Eng. Regen. M.* 4(5), 349–355 (2010).

11   Mandal BB, Kundu SC. Cell proliferation and migration in silk fibroin 3D scaffolds. *Biomaterials* 30(15), 2956–2965 (2009).

12   Kim UJ, Park J, Kim HJ, Wada M, Kaplan DL. Three-dimensional aqueous-derived biomaterial scaffolds from silk fibroin. *Biomaterials* 26(15), 2775–2785 (2005).

▪▪   **The first study that demonstrated that salt-leached silk fibroin scaffolds can be prepared from aqueous silk fibroin solutions.**

13   Mathur AB, Gupta V. Silk fibroin-derived nanoparticles for biomedical applications. *Nanomedicine* 5(5), 807–820 (2010).

14   Oliveira AL, Sampaio SC, Sousa RA, Reis RL. Controlled mineralization of nature-inspired silk fibroin/hydroxyapatite hybrid bioactive scaffolds for bone tissue engineering applications. Presented at: *20th European Conference on Biomaterials.* Nantes, France, 27 September–1 October 2006.

15   Kim HJ, Kim UJ, Kim HS *et al.* Bone tissue engineering with premineralized silk scaffolds. *Bone* 42(6), 1226–1234 (2008).

16   Collins AM, Skaer NJV, Gheysens T *et al.* Bone-like resorbable silk-based scaffolds for load-bearing osteoregenerative applications. *Adv. Mater.* 21(1), 75–78 (2009).

▪▪   **The first study that presented silk/calcium phosphate (CaP) scaffolds with mechanical properties comparable with cancellous bone.**

17   Zhang Y, Wu C, Friis T, Xiao Y. The osteogenic properties of CaP/silk composite scaffolds. *Biomaterials* 31(10), 2848–2856 (2010).

▪▪   **This study demonstrated that silk/CaP scaffolds had osteogenic properties, and promoted the cancellous bone formation in calvarial defect in a rat model.**

18   Yan LP, Oliveira JM, Oliveira AL, Caridade SG, Mano JF, Reis RL. Macro/micro porous silk fibroin scaffolds with potential for articular cartilage and meniscus tissue engineering applications. *Acta Biomater.* 8(1), 289–301 (2012).

▪▪   **This study demonstrated that salt-leached silk fibroin scaffolds can be prepared by**

using aqueous silk fibroin solutions of more than 10 wt.% concentration.

19   Jin H, Kaplan DL. Mechanism of silk processing in insects and spiders. *Nature* 424(6952), 1057–1061 (2003).

20   Kokubo T, Takadama H. How useful is SBF in predicting *in vivo* bone bioactivity? *Biomaterials* 27(15), 2907–2915 (2006).

21   Oliveira JM, Silva SS, Malafaya PB, *et al.* Macroporous hydroxyapatite scaffolds for bone tissue engineering applications: physicochemical characterization and assessment of rat bone marrow stromal cell viability. *J. Biomed. Mater. Res. A.* 91A(1), 175–186 (2009).

22   Dorozhkin SV. Amorphous calcium (ortho) phosphates. *Acta Biomater.* 6(12), 4457–4475 (2010).

23   Lu Q, Hu X, Wang XQ *et al.* Water-insoluble silk films with silk-I structure. *Acta Biomater.* 6(4), 1380–1387 (2010).

24   Chen X, Shao ZZ, Knight DP, Vollrath F. Conformation transition kinetics of *Bombyx mori* silk protein. *Proteins* 68(1), 223–231 (2007).

25   Oliveira JM, Rodrigues MT, Silva SS *et al.* Novel hydroxyapatite/chitosan bilayered scaffold for osteochondral tissue-engineering applications: scaffold design and its performance when seeded with goat bone marrow stromal cells. *Biomaterials* 27(36), 6123–6137 (2006).

26   Oliveira AL, Reis RL. Bone-like apatite coatings nucleated on biodegradable polymers as a way to induce bone mineralization: current developments and future trends. In: *Biodegradable Systems in Medical Functions: Design, Processing, Testing and Applications.* Reis RL, San Roman J (Eds). CRC Press, Boca Raton, FL, USA, 205–221 (2004).

27   Bhumiratana S, Grayson WL, Castaneda A *et al.* Nucleation and growth of mineralized bone matrix on silk-hydroxyapatite composite scaffolds. *Biomaterials* 32(11), 2812–2820 (2011).

■■ **The study demonstrated that the silk/CaP scaffolds enhanced human mesenchymal stem cell osteogenic differentiation *in vitro*.**

28   Kong XD, Cui FZ, Wang XM, Zhang M, Zhang W. Silk fibroin regulated

mineralization of hydroxyapatite nanocrystals. *J. Crystal. Growth* 270(1–2), 197–202 (2004).

29   Karageorgiou V, Kaplan D. Porosity of 3D biomaterial scaffolds and osteogenesis. *Biomaterials* 26(27), 5474–5491 (2005).

30   Oliveira AL, Malafaya PB, Costa SA, Sousa RA, Reis RL. Micro-computed tomography (μ-CT) as a potential tool to assess the effect of dynamic coating routes on the formation of biomimetic apatite layers on 3D-plotted biodegradable polymeric scaffolds. *J. Mater. Sci. Mater. M.* 18(2), 211–223 (2007).

31   Liu L, Liu JY, Wang MQ *et al.* Preparation and characterization of nano-hydroxyapatite/silk fibroin porous scaffolds. *J. Biomater. Sci. Polym. Ed.* 19(3), 325–338 (2008).

32   Rajkhowa R, Gil ES, Kluge J *et al.* Reinforcing silk scaffolds with silk particles. *Macromol. Biosci.* 10(6), 599–611 (2010).

33   Yan LP, Wang YJ, Ren L *et al.* Genipin-cross-linked collagen/chitosan biomimetic scaffolds for articular cartilage tissue engineering applications. *J. Biomed. Mater. Res. A.* 95A(2), 465–475 (2010).